PHILOSOPHICAL TRANSACTIONS A

rsta.royalsocietypublishing.org

Review

Cite this article: Schaller MF, Fung MK. 2018 The extraterrestrial impact evidence at the Palaeocene–Eocene boundary and sequence of environmental change on the continental shelf. *Phil. Trans. R. Soc. A* **376**: 20170081. http://dx.doi.org/10.1098/rsta.2017.0081

Accepted: 30 July 2018

One contribution of 11 to a discussion meeting issue 'Hyperthermals: rapid and extreme global warming in our geological past'.

Subject Areas:
geochemistry, climatology, oceanography

Keywords:
Palaeocene–Eocene Thermal Maximum, extraterrestrial impact, impact ejecta, hyperthermal, carbon cycle

Author for correspondence:
Morgan F. Schaller
e-mail: schall@rpi.edu

The extraterrestrial impact evidence at the Palaeocene–Eocene boundary and sequence of environmental change on the continental shelf

Morgan F. Schaller and Megan K. Fung

Earth and Environmental Sciences, Rensselaer Polytechnic Institute, Troy, NY, USA

MFS, 0000-0003-2742-2126

We have identified clear evidence of an extraterrestrial impact within the onset of the carbon isotope excursion (CIE) that defines the Palaeocene–Eocene (P-E) boundary hyperthermal event (approx. 56 Ma) from several sites on the eastern Atlantic Coastal Plain and offshore. We review and update the state of the evidence for an impact at the P-E boundary, including a K-Ar cooling age of the ejecta that is indistinguishable from the depositional age at the P-E, which establishes the ejecta horizon as an isochronous stratigraphic indicator at the P-E. Immediately above the ejecta peak at the base of the coastal plain Marlboro Clay unit, we identify a sharp increase in charcoal abundance coincident with the previously observed dramatic increase in magnetic nanoparticles of soil pyrogenic origin. We therefore revisit the observed sequence of events through the P-E boundary on the western Atlantic Coastal Plain, showing that an extraterrestrial impact led to wildfires, landscape denudation and deposition of the thick Marlboro Clay, whose base coincides with the spherule horizon and CIE onset. The Sr/Ca ratio of the spherules indicates that the carbon responsible for the onset may be vaporized $CaCO_3$ target rock mixed with isotopically light carbon from the impactor or elsewhere. Crucially, we do not argue that the impact was responsible for the full manifestation of

THE ROYAL SOCIETY PUBLISHING

the CIE observed globally (onset to recovery approx. 170 kyr), rather that a rapid onset was triggered by the impact and followed by additional carbon from other processes such as the eruption of the North Atlantic Igneous Province. Such a scenario agrees well with recent modelling work, though it should be revisited more explicitly.

This article is part of a discussion meeting issue 'Hyperthermals: rapid and extreme global warming in our geological past'.

1. Introduction

The Palaeocene–Eocene (P-E) boundary (56.0 Ma; Gradstein & Ogg [1] time scale) is marked by the onset of a carbon isotope excursion (CIE) observed globally [2]. This global decrease in marine $\delta^{13}C$ was first described by Kennet & Stott [3] in association with a benthic foraminifera extinction at Site 690 in the Southern Ocean. The rapid $\delta^{13}C$ excursion is observed in organic and inorganic marine and terrestrial carbon reservoirs [4], and is associated with marine plankton excursion taxa [5–7], and changes in mammal and plant assemblages [8,9]. Accompanying the CIE is an approximately 5°C global warming and rapid widespread ocean acidification [10,11]. The proposed causes for this event are numerous: dissociation of methane clathrates [12,13], eruption of the North Atlantic Igneous Province (NAIP) [14] or its intrusion into hydrocarbon reservoirs [15], and an extraterrestrial impact [16,17], among many others. However, the extraterrestrial impact ejecta discovered by Schaller *et al.* [18] and summarized here is the first physical evidence of any proposed forcing mechanism for the onset of the climate perturbation that is directly tied to the CIE at the P-E boundary by stratigraphic superposition and radiometric means.

Wright & Schaller [19] provided the first ultra-high-resolution stable carbon and oxygen isotope record through the onset of the CIE, and further suggested that the onset was decadal in scale based on cyclic sedimentary features in the Marlboro Clay unit, which contains the P-E boundary on the North American Atlantic Coastal Plain. Though this was met with significant criticism [20–22], it prompted a much more intense look at the CIE interval in the basal Marlboro Clay. While extracting foraminifera from the CIE onset of these shelf cores (figure 1), Schaller *et al.* [18] serendipitously found impact ejecta (glass spherules) in a discrete horizon coincident with the CIE onset (figure 1). In that study, we used two cores spanning the P-E boundary on the Atlantic Coastal Plain (ODP 174AX—Wilson Lake B and Millville), natural P-E boundary exposures near Medford, NJ, as well as open ocean ODP Hole 1051B (approx. 2000 m water depth). Spherules from each site have the same basic composition and meet all criteria of impact ejecta from known strewn fields, including splashform morphologies, surficial microcraters, low volatile content, related major element chemistries, and shocked quartz and lechatelierite inclusions (figure 2).

Here we summarize the published evidence of an extraterrestrial impact associated with the P-E hyperthermal event, and add new evidence that supports an impact scenario for the onset of the excursion, including radiometric dates demonstrating that the cooling age and depositional age of the spherules are indistinguishable. The virtually instantaneous time line provided by the ejecta horizon provides an opportunity to delineate the detailed sequencing of sedimentation, carbon cycle perturbation, and environmental aftermath at a critical juncture in Earth's climate history. In the suggested scenario, we do not attempt to assign the bulk of the Palaeocene–Eocene Thermal Maximum (PETM) hyperthermal and isotope excursion (10^5 year time scale) [23] to an extraterrestrial impact. Rather, we argue based on the chemistry of the spherules that the onset of the CIE could have been driven by an impact through the vaporization of $CaCO_3$ target rocks mixed with cometary carbon, where the bulk of the carbon constituting the remainder of the event was likely to have been sourced from one or more reservoirs activated by the impact (e.g. increased NAIP activity), or simply coincident with it. We also address post-impact evidence that indicates wildfires occurred across a significant region of East–Central North America immediately following the impact.

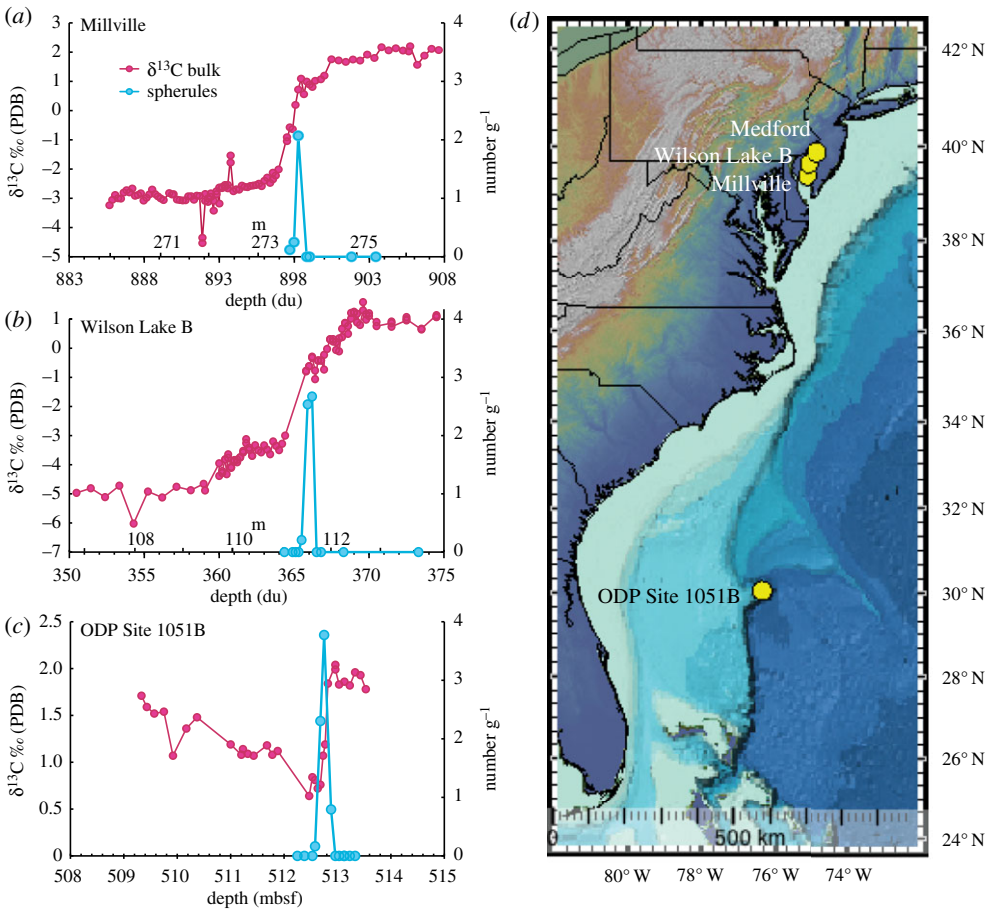

Figure 1. Stratigraphic distribution of P-E spherules from Millville (*a*), Wilson Lake B (*b*), and ODP Hole 1051B (*c*) (modified from Schaller *et al.* [18]). The Millville and Wilson Lake B core depths are indicated in drilling units (du) of decimal feet; core depth in Hole 1051B is in metres below seafloor (mbsf). The bulk carbonate $\delta^{13}C$ from Millville and Wilson Lake B is from Wright & Schaller [19], and Hole 1051B from Katz *et al.* [13]. (*d*) Map showing Atlantic margin locations, including exposure in Medford, NJ, and Site 1051, Blake Nose. Ejecta in the Mid-Atlantic palaeo-continental shelf sites are found in the basal Marlboro Clay Formation.

2. Review of initial observations of impact ejecta in Palaeocene–Eocene sections on the Atlantic Coastal Plain

Detailed stratigraphic and geochemical analyses establish that the material recovered from several P-E boundary sections on the Atlantic Coastal Plain and open ocean are definitively impact ejecta [18]. We summarize the relevant observations. Ejecta from known impact strewn fields have common features that provide useful criteria for identifying previously undiscovered impact ejecta in the geological record. An ejecta deposit typically results from an air-fall event and occurs in a discrete stratigraphic layer. Spherules are generally glasses (microtektites) and may contain crystallites (microkrystites); both have characteristic morphologies and may be either solidified melt ejecta or vapour condensates [24–26]. Microkrystites show distinct internal crystallite textures that indicate rapid quenching from a high temperature; if formed as a vapour condensate, they can be enriched in projectile material depending on the conditions of condensation [26]. Microtektites that form as melt droplets solidify at slightly lower temperatures and are more likely to be vesicular; they may contain inclusions of high-temperature components such as lechatelierite, a quartz glass that solidifies above 1750°C, with a boiling point greater

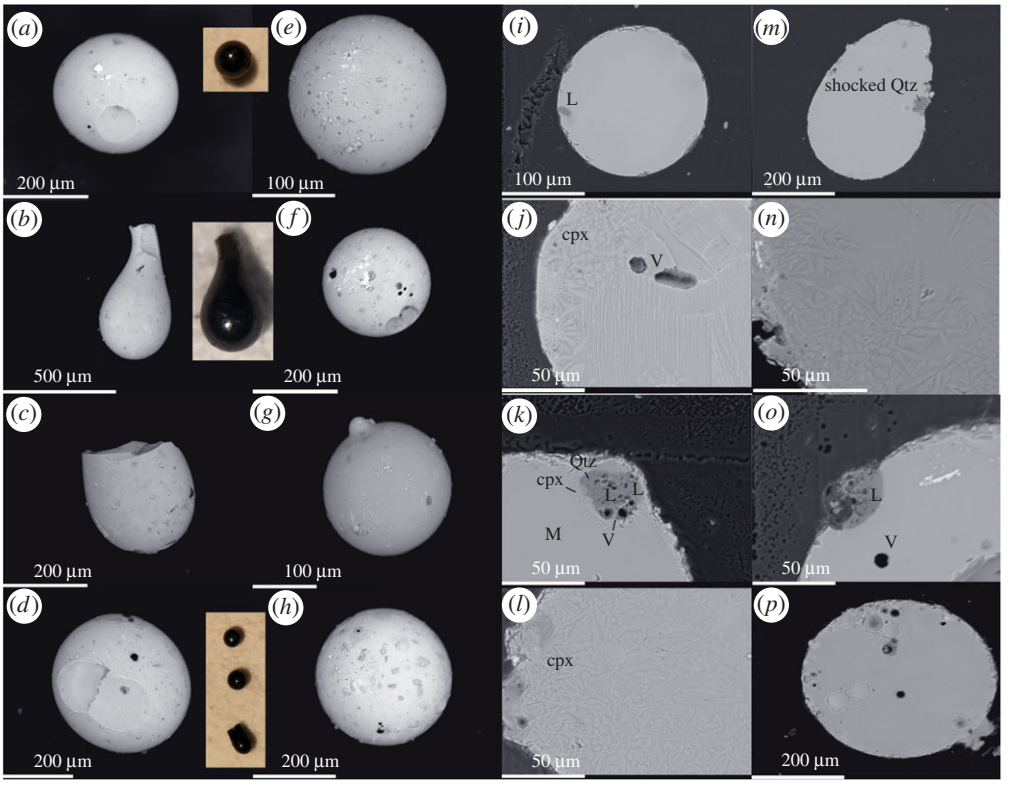

Figure 2. Electron backscatter (15 kV) images of some representative P-E spherules (microtektites and microkrystites) from Hole 1051B, Wilson Lake B, and Millville cores (modified from Schaller *et al*. [18]). Insets are light micrographs. (*i–p*) show P-E boundary spherule cross sections mounted in epoxy (modified from Schaller *et al*. [18]). Note the classic dendritic quench textures. Shocked quartz grain in (*m*) is shown in detail in figure 6. See Schaller *et al.* [18] for details. (Online version in colour.)

than 2200°C [27,28]. The spherules we discovered and detailed in Schaller *et al*. [18] are most likely melt-droplet-type ejecta, based in part on criteria outlined below. As discussed later, melt-droplet-type microtektites and microkrystites are more useful for delineating the source crater location because both ejecta layer thickness and spherule size vary as a function of distance from the point of impact.

(a) Spherules and strata from Palaeocene–Eocene boundary sections

Schaller *et al*. [18] examined three marine P-E boundary sections that encompass the CIE onset [2] (figure 1): continental shelf sites Wilson Lake B (ODP Leg 174AX; 39.6598° N, 75.04717° W) [29] and Millville (ODP Leg 174AX; 39.4046° N, 75.08888° W) [30], where the CIE onset coincides with the base of the thick Marlboro Clay of the Salisbury Embayment (figure 3); and pelagic sediments at ODP Hole 1051B at Blake Nose (30.0531° N, 76.3578° W, water depth 1980.6 m) [33]. To constrain the stratigraphic level of CIE onset, we use detailed bulk sediment $\delta^{13}C$ records from Wilson Lake B and Millville [19], and Hole 1051B [13].

At all three of the localities originally reported by Schaller *et al.* [18], peak spherule abundances occur close to the P-E boundary as constrained by the $\delta^{13}C$ decrease in bulk sediment (figure 1). Spherules are found over a *ca* 20 cm interval at each site, with the number of spherules increasing sharply up-section from zero below to a peak at or close to the P-E boundary. Maximum abundances in the greater than 63 µm size fraction are 2.5–3 spherules g^{-1} at Wilson Lake B and Millville, and 4 spherules g^{-1} at Hole 1051B, followed by a decline in abundance to zero over approximately 10 cm. At Wilson Lake B and Millville, peak spherule abundance coincides with

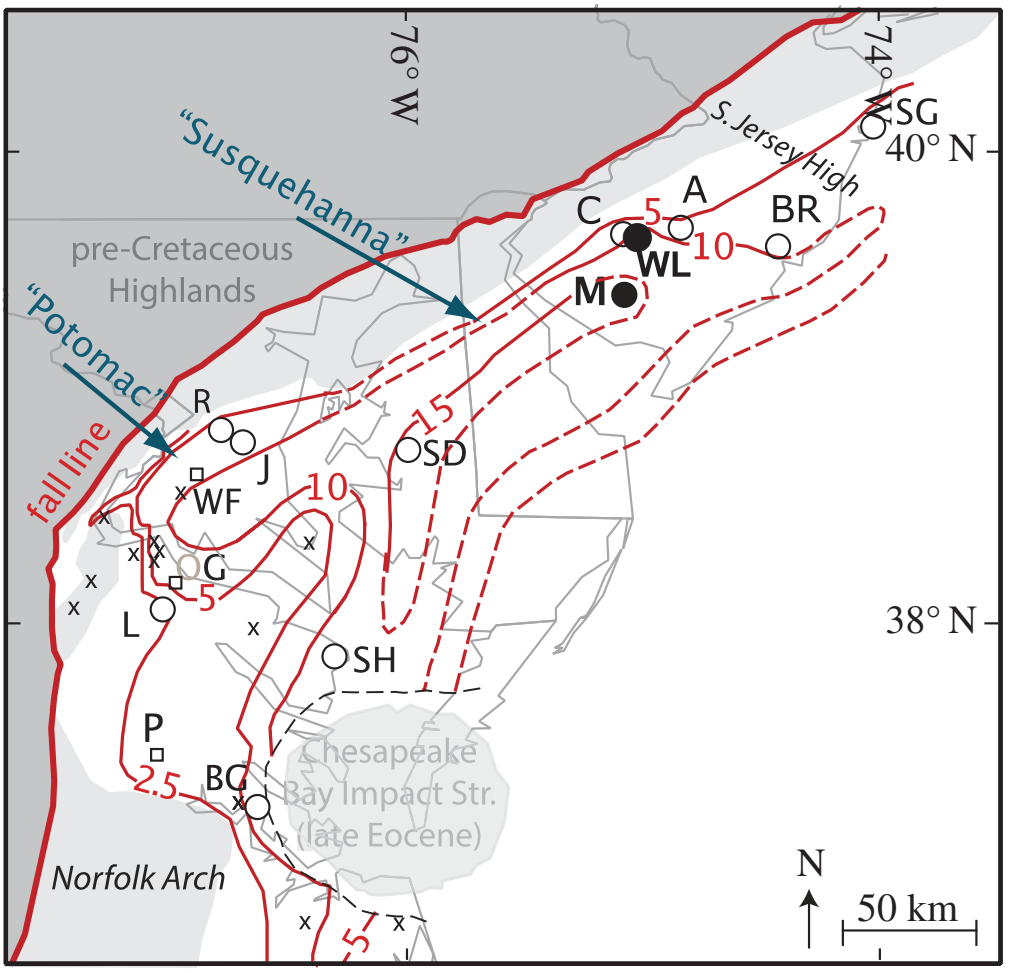

Figure 3. Location map showing distribution of sites along the Mid-Atlantic Salisbury Embayment on the palaeo-continental shelf (modified from Kent *et al.* [31] and Kopp *et al.* [32]). Sites discussed in the text: M, Millville; WL, Wilson Lake-B. Thick red line shows the fall line; thin red contours are the approximate thickness of the Marlboro Clay. Circles represent other core locations with characteristic single-domain magnetic nanoparticles within the Clay unit [32]. 'Potomac' and 'Susquehanna' represent the approximate location of the drainage outlets of these major river systems in the latest Palaeocene. (Online version in colour.)

the basal contact of the Marlboro Clay unit, which is gradational with some reworking of the underlying Vincentown Formation facies. Importantly, the spherules are found within the onset of the CIE at open ocean site 1051B in approximately 2000 m water depth, pointing to air-fall as their depositional origin. Morphologically similar material that has been weathered to clays has been identified by the authors in ODP Leg 165 Hole 999 in the Caribbean.

These impact spherule abundances are similar to those found in distal ejecta layers linked to other extraterrestrial impacts, such as the Late Eocene clinopyroxene (cpx)-bearing spherule layer that emanated from the Popigai impact crater [34–36]. Similar concentrations are found in the Late Eocene cpx spherules at ODP Site 738 in the southern Indian Ocean (approx. 2 spherules g^{-1} (greater than 150 µm)), ODP Site 689 in the Southern Ocean (approx. 5–6 spherules g^{-1} (greater than 63 µm); see [34] for a review); and at Massignano, Italy (approx. 4 spherules g^{-1} (greater than 150 µm) [37]).

The glass spherules from Wilson Lake B and Millville range from 65 to 500 µm diameter (average 302 µm), whereas those at Hole 1051B average 274 µm diameter. The colourless to dark brown/black particles are mostly spherical with rotational morphologies, as well as other

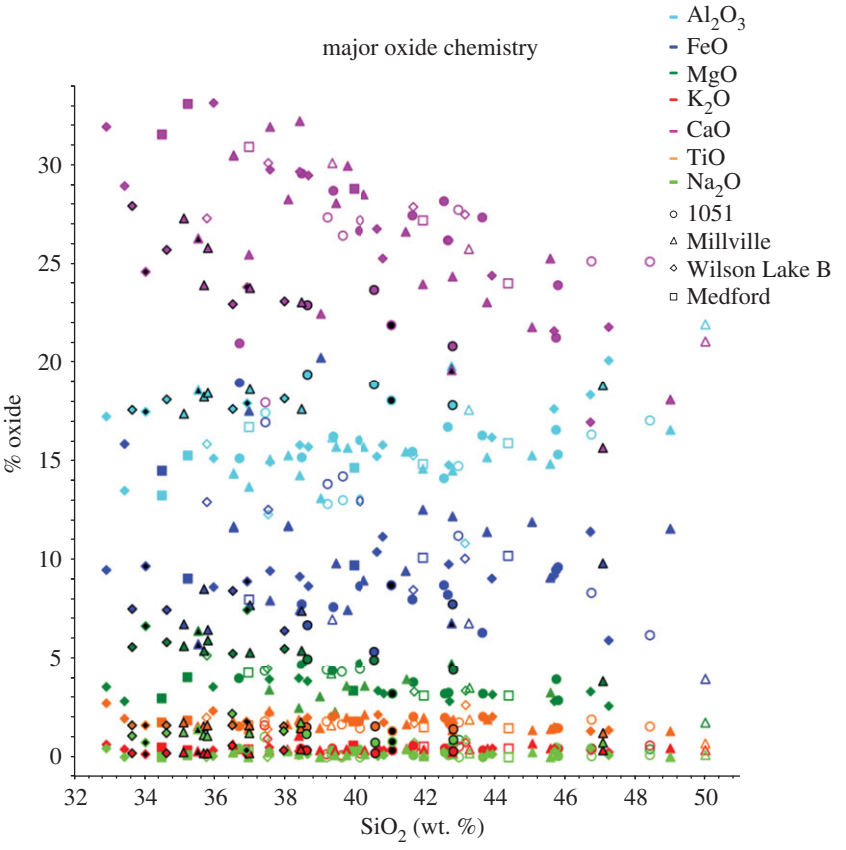

Figure 4. Microtektite and microkrystite major oxide chemistry from Wilson Lake B, Millville, Medford, and Hole 1051B using EDS (modified from Schaller *et al*. [18]) and WDS (this study). Closed symbols represent microtektites, and open symbols denote microkrystites. WDS measurements are shown in black, with a black rim for microtektites and a black interior for microkrystites.

characteristics of splash-form microtektites [24,38] (figure 2). The spherules often have surface pits (figure 2*a*,*b*) and microcraters (figure 2*d*), indicating relative velocities high enough to fracture the solidified glass spherules on impact with one another or other objects. Such microcraters would be unexpected in volcanic spherules. The more shallow surface craters may also be spalation features, where flakes of glass are broken off due to internal stresses when a very hot glass spherule impacts water. There are also occasional broken dumbbell forms (figure 2*c*) and smaller spherules accreted to larger ones (figure 2*g*), often of different chemical composition (figure 2*k*), suggesting they were sintered to one another in a molten state and quenched rapidly. Schaller *et al*. [18] conclude that the stratigraphic distribution and morphologies of the spherules are wholly consistent with an air-fall sedimentary event such as an impact ejecta bed, modified by typical post-depositional bioturbation of marine sediments.

Major oxide chemistries of the P-E spherules show a wide range of compositions distributed equally among Wilson Lake B, Millville and Hole 1051B [18] (figure 4). The CaO content of the spherules (approx. 20–35%) is consistent with a $CaCO_3$-rich target rock (discussed below), with Al_2O_3 (approx. 15%) and FeO (approx. 10%) as the second and third most abundant oxides. This variability is typical of known tektite strewn fields and consistent with an impact origin for the spherules [39,40]. These major element chemistries are confirmed more precisely by wavelength dispersive X-ray spectroscopy (WDS) (figure 4; table 1). Because impact melts have little time for homogenization, a population of major oxide chemistries will generally follow broadly linear compositional trends with SiO_2 content because they were generated from the same source rocks

Table 1. Major oxide chemistry of microtektites and microkrystites measured by WDS and shown in figure 5. Electron High Tension (EHT) is set at 15 kV.

	SiO_2	Al_2O_3	FeO	MgO	K_2O	CaO	TiO_2	Na_2O
microkrystite								
1051 36-37 AL	41.07	18.05	8.69	3.15	0.30	21.90	1.28	0.74
MV 898.5 AM	42.76	19.82	6.79	4.72	0.23	19.62	1.35	0.81
MV 898.8 AM	35.53	18.56	5.71	6.38	0.25	26.31	1.51	1.38
WL 365.5 BV	34.04	17.47	9.66	6.63	0.14	24.62	1.58	0.72
WL 365.5 BW	36.90	17.89	8.89	7.46	0.12	23.84	1.76	0.33
microtektite								
1051 36-37 AJ	40.58	18.87	5.33	4.91	0.18	23.66	1.54	0.72
1051 36-37 AI	38.62	19.41	6.67	4.96	0.31	22.90	1.49	1.14
1051 36-37 AK	42.79	17.83	7.72	4.39	0.27	20.86	1.36	0.84
1051 36-37 AM	22.29	19.38	10.07	7.02	0.06	30.49	3.08	0.60
MV 898.5 AN	38.47	17.62	7.39	5.39	0.36	23.04	1.45	1.72
MV 898.8 AP	35.70	18.24	8.49	5.36	0.19	23.90	1.52	1.07
MV 898.8 AQ	47.06	18.81	9.82	3.80	0.32	15.64	1.20	0.71
MV 898.8 AI	37.00	18.63	7.71	5.29	0.19	23.79	1.57	1.18
MV 898.8 AL	35.80	18.43	6.45	5.91	0.19	25.81	1.57	1.03
MV 898.8 AN	35.13	17.39	6.72	5.64	0.22	27.29	1.71	1.25
WL 365.9 AQ	34.62	18.08	7.46	5.80	0.19	25.73	1.57	1.17
WL 365.9 AR	33.65	17.58	7.49	5.58	0.18	27.94	1.57	1.02
WL 365.5 CA	36.51	17.64	8.41	5.23	0.56	22.97	1.57	2.15
WL 365.5 BU	37.98	18.14	6.37	5.49	0.33	23.11	1.52	1.28

at the site of impact [39]. In contrast, ashes or spherules of volcanic origin tend to exhibit close inter- and intra-spherule compositional homogeneity [40], because lava is generally well mixed during a single eruptive event. Volcanic spherules from the same eruptive sequence will be compositionally homogeneous such that the glasses are representative of the bulk composition. Volcanic glasses also generally have much higher water content than impact spherules (up to a few weight % [41]). In contrast, water content of impact glasses is much lower than volcanic spherules [42,43] because water is removed by vapour stripping during solidification [44]. Fourier transform infrared spectroscopy (FTIR) of the P-E spherules reveals water contents less than 0.023 wt.%, much lower than expected for volcanic spherules, but typical of impact-generated microtektites [18].

(b) Glassy and crystalline internal textures and inclusion chemistry

In polished cross-section, the internal texture of many of the P-E spherules is glassy and relatively featureless (figure 2*i*); exceptions are the less common microkrystites (discussed below). The glassy spherules are mildly vesicular and occasionally have microlites just inside the rims. This vesicular nature, and the composition discussed above, is inconsistent with iron or stony micrometeorites, or other types of cosmic spherules, which are generally either chondritic or metallic, and do not show evidence of volatile degassing [45]. Vesicles in the P-E microtektites indicate they probably formed from melt ejecta rather than condensate [46].

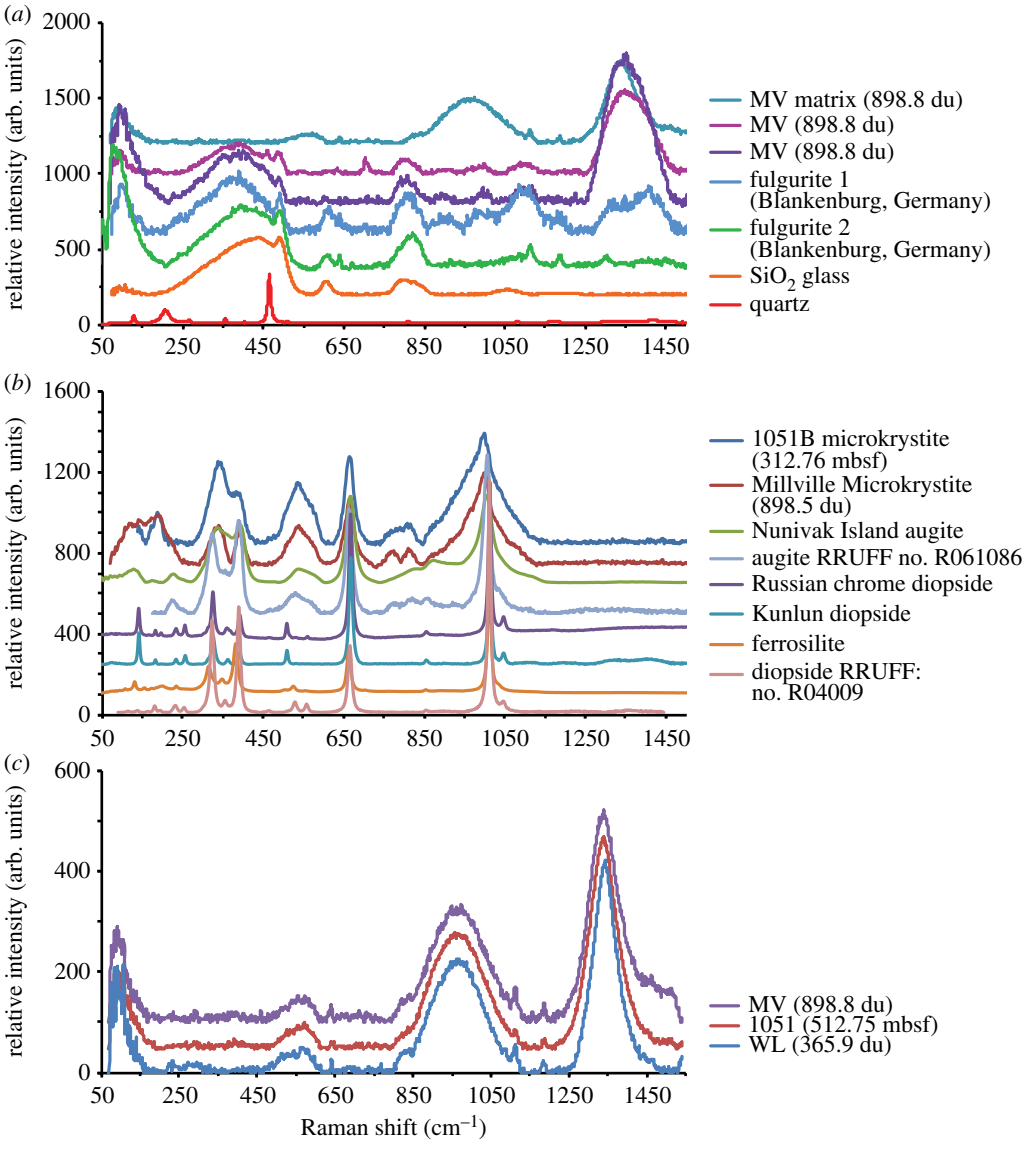

Figure 5. (*a*) Background corrected Raman spectra of representative lechatelierite inclusions found in PE spherules compared with the spherule matrix, lechatelierite from fulgurite, SiO_2 glass, and quartz (modified from Schaller *et al.* [18]). (*b*) Raman spectra of representative clinopyroxene crystallites compared with augite, diopside and ferrosilite standards [18]. (*c*) Micro-laser Raman spectra of representative microtektite matrices. Spectra are collected using a Bruker 532 nm green laser system at the Rensselaer Polytechnic Institute, Troy, NY, and are background corrected [18].

An important observation is the presence of amorphous, occasionally vesicular, nearly pure SiO_2 glass inclusions within the microtektites (figure 2*k*) called lechatelierite, which is a common constituent of impact glasses. Lechatelierite occurrence is confirmed by energy-dispersive X-ray spectroscopy (EDS) and micro-Raman spectroscopy in cross-sections of spherules from Wilson Lake B, Millville and Hole 1051B (figure 5*a*). EDS indicates that these inclusions are greater than 98% SiO_2, with Raman spectra from several that are consistent with fulgurite (lightning-induced lechatelierite). Lechatelierite forms when quartz melts and quenches to quartz glass, which occurs at temperatures greater than 1750°C [27,28] (it boils at 2230°C). This indicates that the P-E spherules formed at temperatures at least this high, which excludes any known terrestrial

volcanism as their origin. Furthermore, melting of crustal silicates by impact sufficient to produce lechatelierite occurs at shock pressures of approximately 30–50 GPa [47,48]. This indicates that the target rock, although not necessarily silica rich, at least had silt-sized or larger quartz grains that melted on impact.

We identified a quartz inclusion in a microtektite from Millville that has Raman spectral characteristics indicative of shocked quartz (figure 6). The relaxation of the spectral peak corresponding to SiO_2 bond-bending vibration from 464 to 460 wavenumbers (cm^{-1}) observed in the Millville spherule inclusion is consistent with observations from synthetic quartz experimentally shocked to peak pressures of 25.8 GPa [49] (figure 6*b*,*d*) and is considered diagnostic. The Millville grain shows additional characteristic spectral shifts unique to shocked quartz. Based on this promising find, we have begun an extensive search for shocked quartz among abundant quartz grains on the shelf. At the time of writing, we have identified another shocked quartz grain at 898.8 feet in the Millville core, out of 200 grains analysed from each sample thus far (figure 6*a*).

A subset of spherules shows quench-crystallization textures of clinopyroxene (figure 2*j*,*l*) (Raman spectra most closely matching augite or diopside (figure 5*b*), in an otherwise glassy matrix (figure 5*c*)), typical of microkrystites [26,50]. The feathered, dendritic and chain-like textures of the P-E microkrystites are classic rapid-crystallization high-temperature quench features seen in impact glasses with lower silica content from other strewn fields. Examples include (i) late Eocene cpx microkrystites [38,51,52] attributed to the Popigai impact [34,36,53] and (ii) K-Pg spherules (discussed below) [54]. Among our P-E microkrystites, vesicles are present but less common. Crucially, the presence of vesicles and lack of Ni-rich spinels in the P-E microkrystites are consistent with melt ejecta, but probably not vapour condensate.

Within each P-E spherule the crystallite chemistry is close to the surrounding glass matrix, with the exception of Fe-rich or Si-rich inclusions. The distribution of major oxide chemistries is similar to, but quite distinct from, the late Eocene cpx spherules, which, like the P-E spherules, have high CaO contents (averaging only approx. 10 wt.%, which is substantially lower than the P-E spherules). However, unlike the P-E spherules, the late Eocene spherules have compositions much higher in SiO_2 and Na_2O, and lower in Al_2O_3 and FeO [39,52,55]. The P-E microtektites and microkrystites are roughly equally represented at Wilson Lake B, Millville and Hole 1051B.

Schaller *et al*. [18] conclude that the spherule layers at Wilson Lake B, Millville, and ODP Site 1051 (in the open ocean) are best explained as air-fall ejecta (microtektites and microkrystites) generated by an impact at the P-E boundary. Ejecta fall-out occurs over hours or days, implying that the spherule layer could provide the most precise isochronous feature for the P-E boundary among the three sites.

3. Additional impact evidence

Additional lines of evidence that are consistent with an impact at the P-E boundary are reviewed below. These include K-Ar and Ar-Ar ages that centre around 55 Ma, the presence of Ni-enriched spinel crystal inclusions in the P-E spherules, and evidence for widespread contemporaneous wildfire activity directly above the spherule level at several sites.

(a) Radiometric and cyclostratigraphic determinations of the Palaeocene–Eocene boundary age

The P-E boundary is marked by the onset of the CIE [2]. However, the CIE onset can be offset in bulk sediments and foraminifera measured in the same samples [56]. The age of the P-E boundary has been estimated by integrating radiometric dates on earliest Eocene ashes with cyclostratigraphy [57–59]. Therefore, the exact age of the CIE onset is not known by absolute

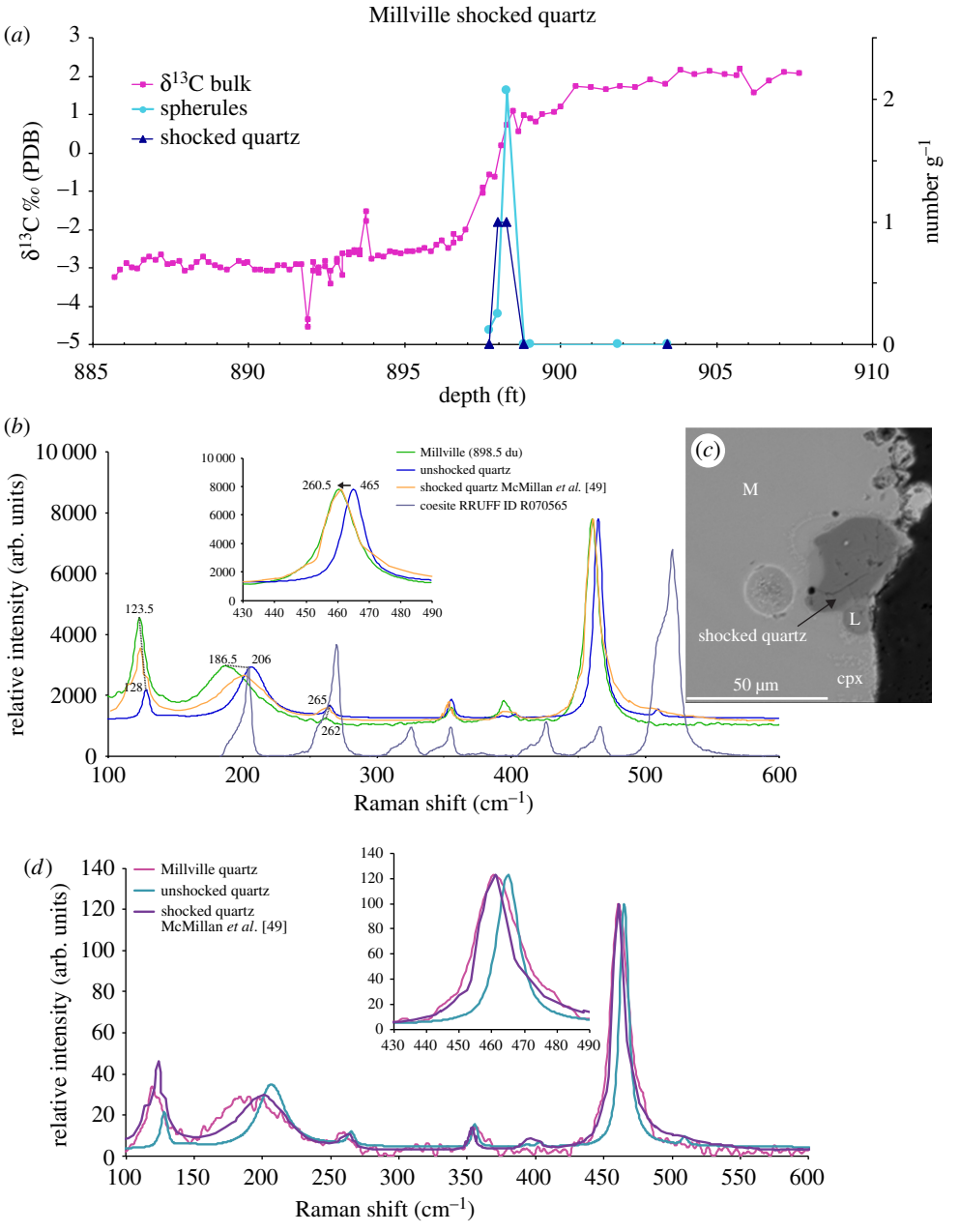

Figure 6. (*a*) Distribution of the shocked grains with depth, compared with the spherule peak and the CIE. At present only 200 quartz grains from each sample at Millville were analysed for shock metamorphism. (*b*) Background corrected Raman spectrum of a polished microkrystite containing crystalline quartz (Millville 898.5 du) and an unshocked quartz standard [18]. Black dashed lines note shifts in various vibrational modes between an unshocked quartz grain and the quartz inclusion in the microkrystite. These measurements are compared with spectra for quartz shocked to peak pressures of 25.8 GPa [49], which are remarkably consistent with those from the Millville inclusion. Inset shows characteristic 464 to 450 wavenumber vibrational relaxation associated with shocked quartz. (*c*) Electron backscatter image of a polished microkrystite from Millville containing the shocked quartz grain analysed in (*b*). Scale bar = 50 µm [18]. L, lechatelierite; M, matrix; cpx, clinopyroxene microlites. (*d*) Raman spectra of the shocked grain at 898.8 du (pink) compared with synthetically shocked quartz from McMillan *et al.* [49] (purple).

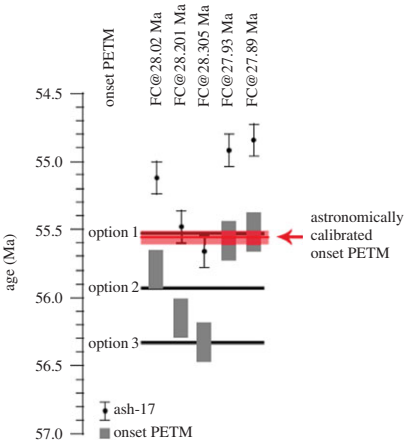

Figure 7. Age estimates for the onset of the Palaeocene–Eocene CIE (modified from Westerhold *et al.* [57]). The different ages of the Fish Canyon Tuff Ar-Ar standard yield different ages for the P-E boundary.

dating techniques, and because of Solar System chaos and the differences between the accepted ages of the Fish Canyon Tuff (FCT) (see discussion in [57,60]), a range of absolute age options are given from 55.53 to 56.3 Ma (figure 7). The basis for these ages are ^{40}Ar-^{39}Ar dates from an ash in the Fur Formation that Storey *et al.* [14] correlate to the '−17 ash' in site 550, from which Westerhold *et al.* [57,58] used cyclostratigraphy to determine the age of 55.53 ± 0.05 Ma for the CIE onset for that site. However, both the −17 and +19 ashes fall well above the recovery of the CIE, and hence do not put an absolute age on the boundary itself.

Charles *et al*. [59] date zircons from a bentonite found in the 'core' of the CIE at Spitsbergen, Norway, to 55.785 ± 0.086 Ma by U-Pb, which they use to cyclostratigraphically constrain the CIE onset to 55.866 ± 0.098 Ma. As far as we are aware, this U-Pb dated bentonite is stratigraphically the closest published date to the CIE onset, and appears to agree with Westerhold *et al*.'s [58] age for the boundary calculated from an FCT age of 28.02 Ma (figure 7, 'option 2'). Jaramillo *et al*. [61] used U-Pb on zircons to date a pyroclastic tuff at the level of a CIE on the Venezuelan coastal plain to 56.09 ± 0.03 Ma, which is suggested to be the onset of the P-E CIE. However, the CIE does not manifest in its typical form at this site, and the 'tuffaceous sandstone' containing the zircons appears to be above the onset of the CIE, within the excursion body. It is possible that this ash layer is reworked, which would explain the discrepancy between the Charles *et al*. [59] and Jaramillo *et al*. [61] dates.

(b) K-Ar and ^{40}Ar-^{39}Ar ages of the Palaeocene–Eocene microtektites

The microtektites in the CIE onset [18] (figure 1) provide an opportunity to radiometrically date the P-E boundary directly using ^{40}Ar-^{39}Ar. Although it is currently unlikely that we can immediately address the P-E 'dating dilemma' proposed by Westerhold *et al*. [57], because the precision on tektite-derived dates may be outside the bounds necessary to significantly revise the age of the onset of the CIE (for example, see figure 7), it is still important to establish that the cooling age of the spherules is equivalent to their depositional age. Work on refining the precision of microtektite ^{40}Ar-^{39}Ar dates using a larger population of grains is ongoing and so the current state of our knowledge is discussed here.

Because the K-content of the P-E spherules is so low (generally less than 0.5 wt%), and their sizes relatively small, dating individual grains by ^{40}Ar-^{39}Ar is an analytical challenge. However, a K-Ar date, and a suite of successful Ar-Ar dates [62,63] reveal a cooling age of approximately 55.4 Ma, which is consistent with the depositional age at the P-E boundary. Because the ^{40}Ar-^{39}Ar data are currently under review elsewhere, we describe the K-Ar age here. A

single spherule of relatively high K-content (0.197% K by weight) was brought to total fusion in a high-vacuum extraction line and let into the analyser chamber of a calibrated quadrupole mass spectrometer (QMS) at Rensselaer Polytechnic Institute, Troy, NY (RPI). The total amount of ^{40}Ar was determined to be 2.25×10^{-15} moles. Based on WDS measurements from the electron microprobe (described above), the K content of this spherule was 0.197%. We use the fraction of ^{40}K that decays to ^{40}Ar of $\lambda/\lambda_e = 9.54$, and assume no initial ^{40}Ar. Given the error on our total K measurement, and the inherent inaccuracy of the ^{40}Ar determination on the QMS (5% reproducibility on 10^{-15} moles ^{40}Ar), we place a 3 million year error on our preliminary age of 54.9 $\pm$3 Ma. This age is consistent with ^{40}Ar-^{39}Ar results on the ejecta spherules that cluster around 55.4 Ma [62,63].

The K-Ar age of *ca* 54.9 $\pm$ 3 Ma is crucial for two important reasons: (i) it demonstrates that the depositional age is indistinguishable from the cooling age of the spherules; and (ii) it does not support the hypothesis that the spherules are reworked impact material from another event (e.g. K-Pg or similar), establishing a record of extraterrestrial impact at the P-E boundary. Although the error envelope on the K-Ar age does not allow us to completely exclude the possibility that the ejecta is reworked from an impact somewhere in that time window, such a reworking scenario does not explain the presence of the spherules at open ocean site 1051B at a stratigraphically equivalent level within the onset of the CIE. Because the depositional and cooling ages of the spherules appear to be indistinguishable, the spherules may represent an isochronous marker to which other observations at the P-E boundary may be referenced. If we accept the air-fall ejecta deposit as the most isochronous horizon available, we are freed from the need to reference all other observations at the P-E boundary to the onset of the CIE, which is diachronous depending on the response time of the reservoir in question (e.g. [64]). This opens up the new possibility of assessing the true leads–lags in the C-system response between different surficial carbon reservoirs that react and equilibrate on different time scales. For example, one may reasonably expect that the shelves would respond much more rapidly to an atmospheric perturbation than the open ocean [65–67], but the level of resolution in open ocean sections is insufficient to address this directly using the CIE recorded at each site. Referencing the CIE to the ejecta layer will make these effects apparent particularly at high sedimentation rate sites and will be the subject of significant further work.

(c) Spinel inclusions in the Palaeocene–Eocene boundary spherules

The presence of Ni-rich spinel inclusions in ejecta spherules is an indication of impact origin as the spinels are mostly condensates of vaporized projectile material [26]. These grains are unexpected in melt-drop microtektites and microkrystites, but have been reported in Precambrian melt-droplet microkrystites [46]. Ni-rich spinels are common in other extraterrestrial impact spherules, specifically the K-Pg boundary spherules and the upper Eocene cpx spherules [68–71]. Low Ti and high Mg, Al and Ni contents of the cpx spinels are markedly different from terrestrial spinels, as the Ni content of crustal material is generally less than 0.1 wt % [71], suggesting a meteoritic origin [69]. The skeletal, often dendritic nature of the magnetite inclusions at the K-Pg is the result of rapid crystallization from a high-temperature liquid [72].

Iron-rich inclusions are found in a few (less than 15%) of the P-E boundary microkrystites. These inclusions are small (5–15 µm), round or skeletal in appearance, and occasionally lack a clear crystalline structure (figure 8*a*). WDS and Raman spectroscopy confirm that these Fe-rich inclusions are spinels. Raman spectra, collected using a Bruker SENTERRA Raman microscope with a 785 nm laser at RPI, are background corrected and compared with a magnetite and magnesiochromite standard. The spectra are consistent with magnesium–aluminium magnetite (figure 8*d*), confirming that the inclusions are indeed crystalline spinels. Because of their very small size (approx. 10 µm), we were only able to collect conclusive Raman spectra on one of the inclusions (MV 898.8 AJ no. 1).

WDS measurements made using a Cameca SX-100 electron microprobe at RPI on three spinel-bearing spherules are shown in table 2 and are compared with terrestrial magnetite. The spinel

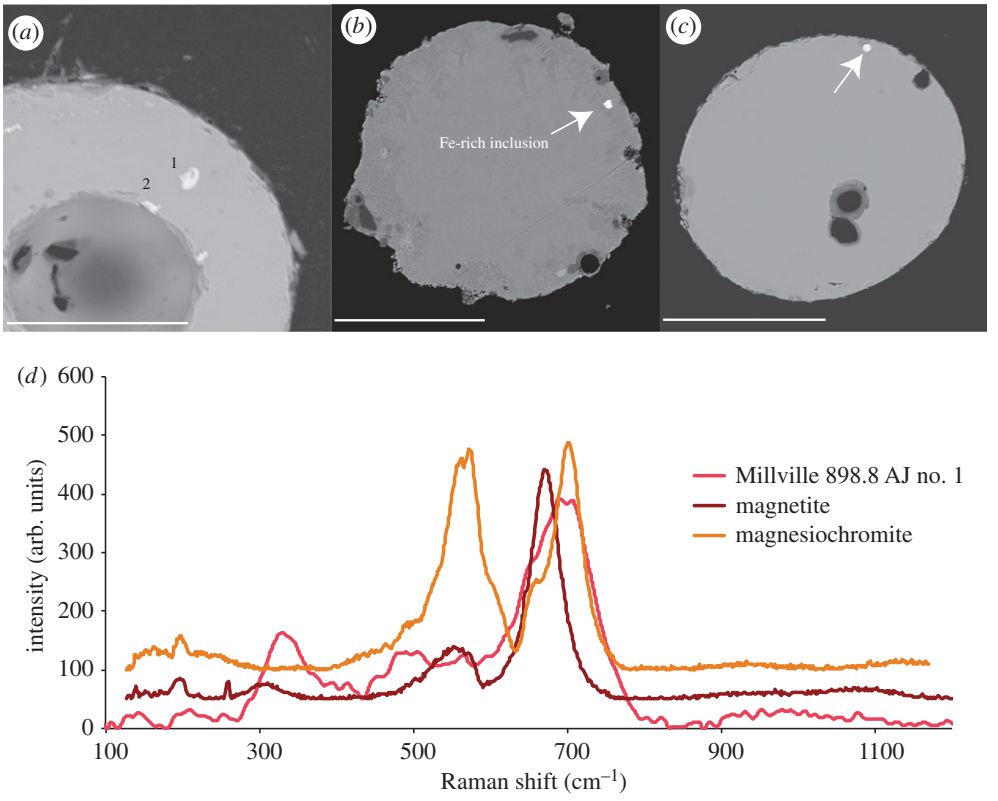

Figure 8. (*a*) Electron backscatter (15 kV) images of the spherules containing Fe-rich inclusions measured in table 2. Scale bar = 200 µm. (*a*) Millville 898.8 AJ. (*b*) Millville 898.8 AM. (*c*) Millville 898.8 AN. (*d*) Raman spectra of an Fe-rich inclusion at Millville 898.8 AJ, compared with standard of magnetite and a reference spectrum of magnesiochromite (RRUFF ID: R050399).

Table 2. Composition of spinel inclusions in three P-E boundary spherules measured by WDS. Two inclusions are measured on MV 898.8 AJ, shown in figure 8*a*. EHT is set at 15 kV. Inclusion measurements (in per cent) are compared with a terrestrial magnetite sample [73].

spherule	Ni	Mg	Al	Si	Ti	Fe	Ca	O	total
MV 898.8 AJ no. 1	0.10	6.01	4.61	0.45	0.20	54.64	0.05	32.24	98.30
MV 898.8 AJ no. 2	0.16	5.07	4.62	0.44	0.24	56.20	0.10	32.35	99.18
MV 898.8 AM	0.03	3.53	3.04	1.04	0.11	61.02	0.11	32.56	101.43
MV 898.8 AN	0.03	1.90	0.33	0.11	0.05	65.24	0.14	29.81	97.63
terrestrial magnetite [73]	—	tr.	0.13	0.24	tr.	73.26	tr.	26.37	100.11

inclusions show variable concentrations of Ni, Mg and Al in the P-E boundary microkrystites, although the two inclusions within the same spherule are most similar. The different contents of these spinels may be a result of varying formation temperatures because the solubility and therefore the incorporation of other elements increases with temperature [74]. The P-E boundary spinels can be distinguished from characteristic basaltic-type spinels by their distinctly low Ti and Cr, and high Mg and Al concentrations [72]. The extraterrestrial source for the spinels is somewhat ambiguous at this time, as only one crystal appears to have Ni content well above a typical terrestrial surface sample. However, the Mg and Al contents are well outside the

range of typical terrestrial spinels. These unusual chemistries are not necessarily indicative of an extraterrestrial origin, but are distinct from terrestrial magnetites and at least one spherule indicates a Ni-enriched source. If the spinel inclusions are indeed of extra-terrestrial origin, they are not indicative of a chondritic projectile.

(d) Ir in Zumaya and elsewhere

High-energy impacts may be sufficient to eject all impactor material off the planet and into space; in such events, we would not expect enrichment of siderophile elements (like Ir) on Earth [75]. We note that high energy does not necessarily indicate a large impact—the impactor could be identified at the P-E boundary a fast moving projectile (like a comet). Nonetheless, a modest Ir anomaly has been identified at the P-E boundary in flysch deposits from Slovenia [76], and in a P-E section at Zumaya, Spain [77], though the anomaly at Zumaya has been interpreted to be volcanic in origin in lieu of other impact evidence at that time [78]. We also note that a large iridium or other platinum group element (PGE) anomaly is not necessarily associated with all major impacts (e.g. absence at the Chesapeake impact [79]). At the P-E boundary in Zumaya, the Ir is concentrated in a centimetre-scale layer just preceding the onset of the CIE. Although course-grained ejecta (e.g. spherules and shocked mineral grains) have yet to be identified at this bathyal site, it could be present near the Ir anomaly. A comprehensive search for PGEs (along with trace element chemistries from the spherules) is currently underway at localities where the spherules have been recovered.

(e) Marquez Dome: possible impact site?

There is currently no identified crater for the P-E boundary strewn field. This is not particularly surprising, as the P-E boundary spherules are a relatively new discovery and not all extraterrestrial impacts have known crater locations. For instance, no impact crater is associated with the Australasian strewn field, despite being the largest and youngest Cenozoic at approximately 0.8 million years ago [80,81]. However, the Marquez Dome impact structure, a buried complex impact crater in eastern Texas (31°16′58″ N, 96°17′42″ W), was stratigraphically dated to be 58 ± 2 Ma [82]. This age was later confirmed to be 58.3 ± 3.1 Ma by apatite fission-track dating on impact breccias [83]. The structure appears to be the remnants of a 12.7 km diameter impact of Palaeocene/Eocene age, with a present surface exposure of 2–3 km [84]. The exposed surface of unconsolidated sand and clays [82] is bound by outcrops of the Palaeocene/Eocene age Calvert Bluff Formation of the Wilcox Group [85]. Better-constrained ages for the Marquez Dome are needed to test whether it is the impact site for the P-E strewn field. Intriguingly, the target rocks in the Marquez crater are Mesozoic shelf carbonates [84], consistent with the 20–35% CaO content and the Sr/Ca of the spherules, discussed below.

4. Wildfires following the impact event

Thermal radiation from an impact event can cause massive wildfires [86,87] and has been documented following the K-Pg impact event [88–90]. Here, we review two independent lines of evidence that point to wildfires following the P-E impact: a spike in charcoal abundance and a coincident increase in isolated single-domain magnetic nanoparticles near the base of the Marlboro Clay, immediately above the spherule layer.

A significant increase in charcoal falls stratigraphically above the peak in P-E spherules at palaeo-continental shelf site Wilson Lake B and decreases up-section [91] (figure 9). The charcoal peak is composed of individual charcoal grains that exhibit the remains of charred plant features (e.g. cellular features) and are consistent with preserved fossilized charcoal [91,94]. A comprehensive treatment of the charcoal data is forthcoming.

An unusual change in magnetic character of the sediments occurring near the base of the Marlboro Clay is documented at multiple Atlantic Coastal Plain sites over an expansive area

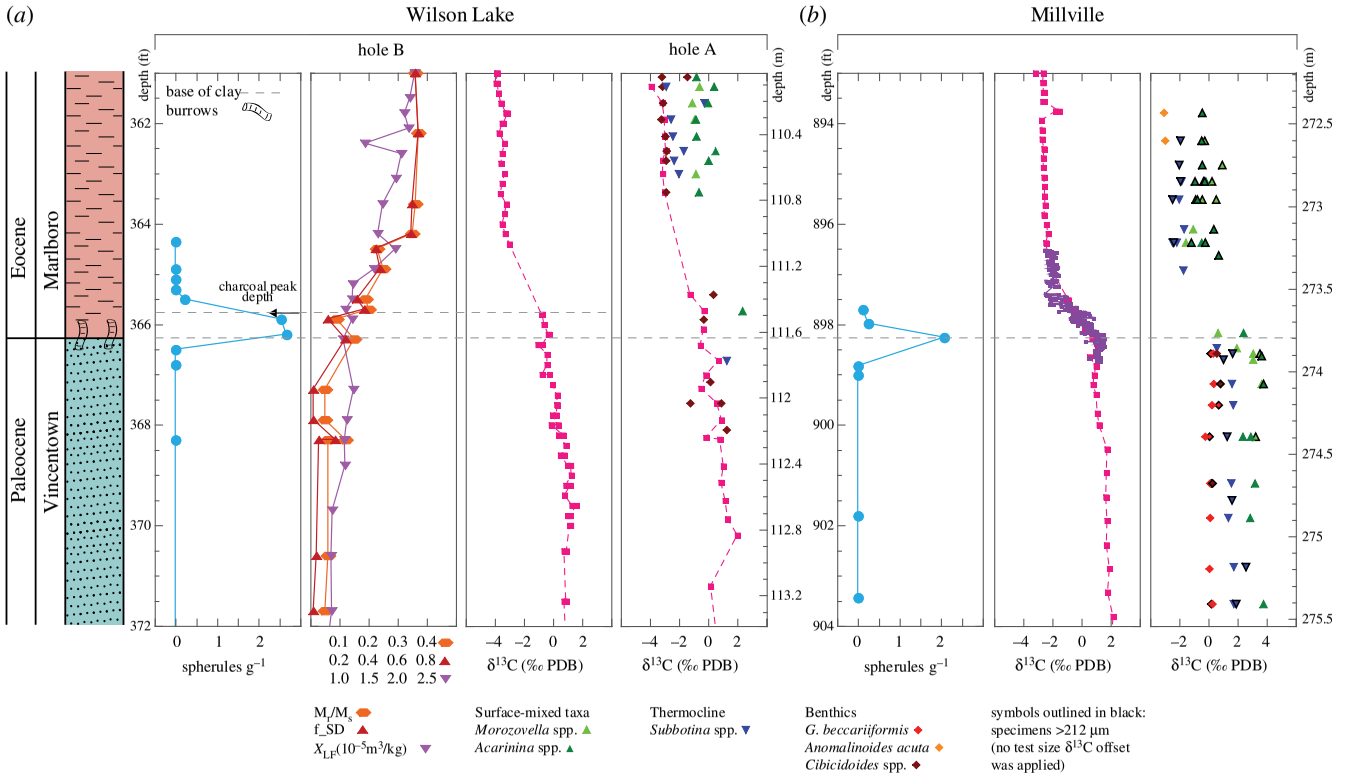

Figure 9. An expanded view of the CIE onset on the palaeo-continental shelf at sites Wilson Lake and Millville demonstrating the order of events at the P-E boundary. Spherule abundance at Wilson Lake B and Millville [18], bulk carbonate $\delta^{13}C$ at Wilson Lake B and Millville [19], bulk carbonate and foraminiferal $\delta^{13}C$ at Wilson Lake A [92], foraminiferal isotopes at Millville [93] and magnetics from Wilson Lake B [93] are shown for comparison. Arrow indicates the depth of the peak in charcoal abundance at Wilson Lake B [94]. The horizontal dashed grey lines identify the apparent offset between an initial decrease in $\delta^{13}C$ measured in bulk carbonate and the spherule peak, which coincides with the base of the Marlboro Clay and defines the start of the CIE onset and P-E boundary (shown in excursion foraminiferal and bulk $\delta^{13}C$ values above). A 5 du depth adjustment is applied to the Wilson Lake A record for comparison with Wilson Lake B. Ratio of saturation remanence to saturation magnetization (Mr/Ms), low-field magnetic susceptibility (XLF) and volume-weighted SD fraction (f_{SD}) at Wilson Lake B from Kent *et al.* [93] illustrates the abrupt rise in magnetization coincident with the peak in charcoal abundance. The foraminiferal isotopes at Millville are not corrected for a $\delta^{13}C$ size offset and samples containing specimens greater than 212 µm are outlined in black. The samples through the onset at Millville are assembled from a number of different sampling campaigns and we note that samples could be shifted up or down *ca* 10 cm due to depletion of the core and shrinkage from their absolute positions.

of the Salisbury Embayment in 11 sites extending from New Jersey to Virginia (approx. 400 km) [16,32,95]. The most recent work points to a pyrogenic origin of the magnetic nanoparticles at Wilson Lake B (figure 9) and Millville [31,96], and similar processes were probably at play in the formation of the unique magnetic assemblage at all of these sites. Saturation magnetization (M_S), low-field magnetic susceptibility (X_{LF}) and other rock magnetic parameters increase dramatically just above the impact spherule layer (figure 9). Soil pyrogenesis caused by wildfires triggered by the P-E boundary impact event provides a plausible scenario for the unique magnetization of the Marlboro Clay [96], and a reservoir of pyrogenically altered soils that can be periodically tapped by erosion. The magnetic and charcoal records combined provide two completely independent lines of evidence indicating that wildfires immediately followed the P-E impact event. The wide aerial extent of the magnetic nanoparticles in the Marlboro Clay suggests that the wildfires covered a significant portion of the Eastern Mid-Continent immediately following the P-E impact.

The base of the Marlboro Clay coincides with the spherule layer at all sites examined so far [18]. Modern wildfires drastically change soil characteristics and erodibility, subsequently intensifying run-off [97] with erosion rates increasing up to 30-fold compared with pre-fire levels [98]. Greatly enhanced sedimentation rates due to these P-E boundary wildfires are likely to be responsible for depositing at least part of the Marlboro Clay unit [91,94,96].

5. The role of an impact in Palaeocene–Eocene climate change

The unprecedented high stratigraphic resolution of the Wilson Lake B and Millville Sites, where the CIE occurs over metres, compared with just a few centimetres in open ocean sites (e.g. Sites 1051 and 690 [99]), gives unprecedented temporal resolution through the event. The nearly instantaneous timeline of the spherule horizon makes it possible to delineate the sequence of sedimentation, carbon release and environmental perturbation in an unusual level of detail. For example, the apparent variable offsets between the ejecta horizon and inflections in the bulk sediment $\delta^{13}C$ records at Wilson Lake B and Millville, compared with the step function in foraminiferal $\delta^{13}C$ [18], can only be viewed at this unfamiliar level of ultra-high resolution. Likewise, the spherule peak coincides with the base of the Marlboro Clay at every site we have examined, followed by a peak in charcoal abundance a short distance above, with a distinct change in magnetic character of the sediments within the same interval (figure 9). This clearly delineates the observed order of events: an extraterrestrial impact, followed by a significant increase in sediment delivery to the shelf, accompanied by multiple lines of evidence suggesting wildfires in the hinterlands. Encased within this short time frame is the onset of the CIE and a climatic warming. Below we review the observed stratigraphic order of events in a level of detail that has so far not been possible from another P-E section, using the spherules as an isochronous horizon. We then speculate on the source(s) of the CIE onset as a consequence of an extraterrestrial impact based on the chemistries of the spherules, and outline a scenario that incorporates the eruption of the NAIP in good agreement with recently published modelling efforts. Finally, we compare the P-E isotope excursion and climate events with the observed changes associated with other large extraterrestrial impacts.

(a) Stratigraphy and order of events with respect to the impact ejecta horizon

If the impact was at least in part responsible for the onset of the CIE, then we expect that the ejecta deposit will appear stratigraphically just before the CIE onset that marks the P-E boundary. The dated air-fall ejecta horizon appears to be isochronous at the base of the Marlboro Clay, with a small smearing effect from bioturbation, and is similarly situated in open ocean site 1051B. Consequently, we use it as the single horizon within the P-E transition strata to which all other observations can be referenced. However, rarely has the onset been scrutinized at this level of detail. At Millville, the spherule peak coincides with the beginning of the CIE onset recorded in the high-resolution bulk $\delta^{13}C$ record of Wright & Schaller [19] (figure 9). We note, however, that there is a gradual $\delta^{13}C$ decrease of approximately 1‰ starting approximately 2 feet (approx.

60 cm) below the spherule peak, prompting the question of whether the CIE began prior to the impact. Recent foraminiferal stable isotope data confirm that the high-resolution bulk $CaCO_3$ records the CIE onset within the base of the clay at Millville, with pre-CIE $\delta^{13}C$ values up to the spherule level and post-CIE values only above it [93] (figure 9). At Wilson Lake A-B, Schaller *et al.* [18] showed that published foraminiferal data remained unchanged to just below the spherule peak, while the bulk carbonate $\delta^{13}C$ decreased by approximately 2‰ starting approximately 2.6 feet (approx. 0.8 m) below the spherule peak (grey vertical lines, figure 9). At both sites the foraminiferal and bulk $CaCO_3$ stable isotope values in the sands are divergent; at Wilson Lake, the bulk and benthic foraminiferal values converge in the clay above the ejecta horizon, while the bulk and thermocline $\delta^{13}C$ values converge in the same interval at Millville. This divergence between the foraminiferal and bulk $CaCO_3$ stable isotope values in the sands, and convergence within the clay indicates that other, more complex, processes are affecting the bulk $CaCO_3$ at this abrupt change in shelf depositional regime. Much more work is needed on this basal interval of the Marlboro, where foraminifera are mostly absent, to more rigorously determine the size and timing of the CIE onset in foraminiferal carbonate relative to the spherule horizon.

An intriguing observation is that the bulk carbonate $\delta^{13}C$ tracks the benthic foraminiferal $\delta^{13}C$ within the clay at Wilson Lake (e.g. [96]), but is divergent from the foraminiferal record within the sands. The total change in $\delta^{13}C$ in benthic foraminifera through the onset at Millville is greater than 3.5‰, which exceeds the benthic change in the open ocean. The absolute $\delta^{13}C$ values before and after the onset of the CIE are also different for each of the foraminifera groups (surface, thermocline and benthic) at Wilson Lake and Millville, pointing to irregular differences in $\delta^{13}C$ of the carbon pools between the two sites. As has been noted by several others, the Marlboro Clay has all the features of shelf clastic units deposited by density-driven hyperpycnal flows or flocculated clay mudwaves [96,100–103]. These types of depositional regimes have been shown to deposit very thick packages of fine-grained sediment on the modern shelf very rapidly [104,105], especially immediately following wildfires [106,107]. It is important to note that density-driven deposition of mud waves is benthic and does not affect the clarity of the water photic zone. These models of sediment deposition are also consistent with the interpretation of a drastic increase in freshwater input to the shelf coinciding with the CIE onset [9,93,100,108]. Given this level of geochemical complexity (compared with the open ocean) and rapid sedimentation, and inadequacy of the current foraminifera record at the base of the clay, it is clear that bulk records should be used with caution when assessing time scales in shelf settings by methods where equilibrium with the open ocean must be assumed, or where an equilibrium response of the surface waters is necessary (e.g. [109]).

(b) Deposition of the unusually thick Marlboro Clay

Several lines of evidence indicate that the sedimentation rate through the Marlboro Clay is likely to be highly non-uniform, where the base was deposited exceedingly rapidly (for example, as suggested by [19], discussed below), while the rest may have been deposited much more slowly [110]. This is consistent with the relative lack of foraminifera in the barren zone of the lower *ca* 50 cm of the clay at multiple localities (e.g. [93,111]), which is followed by a recovery to a higher foraminiferal flux towards the middle of the clay unit [110], discussed below. This is also consistent with the relative lack of bioturbation in the lower one-third of the clay (excluding the transition with the uppermost Vincentown), and resumption of bioturbation toward the middle. A high sedimentation rate at the base is also consistent with observation of a prominent and upright terrestrial plant stem captured by the Wilson Lake B core at approximately 111.7 m (366.6 du) [29,112]. Modern shelf surface waters have been shown to change rapidly in response to a forcing (e.g. greater than 15°C annual temperature swings) and maintain disequilibrium with the open ocean surface waters on long time scales [65–67,113,114]. There is certainly no reason to expect a resumption of normal continental shelf hydrography and quiescent deposition of sediments following an extraterrestrial impact and land clearance by wildfire (e.g. [115,116]).

The main body of the CIE as observed in the open ocean is probably never fully recorded in these proximal shelf sections, all of which show that the Marlboro Clay has been truncated by an unconformity [29,30,32,93]. The classic interpretation of this is that sediment flux is outpacing the available accommodation space on the shelf [117,118], and almost all available sedimentation rate estimates (including those of Stassen *et al*. [110,119] discussed below) induce more sediment than the shelf can accommodate. The foraminiferal isotope data from Millville [93] show a protracted CIE 'core' that occupies the majority of the thickness of the Marlboro (approx. 10 m), followed by a relatively short possible initiation of the recovery phase (approx. 4 m) before an erosional unconformity. Despite the substantial thickness of the P-E transition interval, the full scale of the event is not recorded in these relatively shallow shelf localities, and hence the full *ca* 15 m thickness of the Marlboro Clay at, for example, Millville does not capture the entire *ca* 170 kyr [23] onset through recovery. The exact proportion of the complete event that is recorded by the Marlboro will need to be explicitly evaluated.

Notably, Wright & Schaller [19] argued that the Marlboro Clay contains sedimentary couplets that may be seasonal in origin, and was deposited extremely rapidly. This hypothesis garnered criticism, but reinvigorated discussion on the onset of the CIE. The most significant critique is that the couplets in the Marlboro Clay originate from drilling injection and are not primary sedimentary features [120]. Though not yet published, several auger cores (which do not use drilling mud) and a simple push core were taken through the Marlboro Clay at Medford, NJ, both showing clear expression of the bedding at the same *ca* 1.5–2.5 cm scale [121]. Millimetre-scale grain size measurements and X-rays of the cores show clear sedimentary cyclicity on this scale as well [112]. The bedding is also apparent in what few outcrops are available (e.g. see figure 1 in [21]), despite alternative interpretation of the outcrop evidence as the product of jointing [120]. While drilling injection may have occurred, in lieu of a direct geochemical comparison between the injection features and the drilling fluid used, it is not currently possible to verify this other than by inference. Work on the nature and origin of these deposits is ongoing.

(c) Foraminiferal accumulation rates

Wright & Schaller [19] suggested that the sedimentary cyclicity was seasonal, lending a decadal scale to the onset recorded at the coastal plain sites. This interpretation is contrary to the available foraminifera mass accumulation rate (MAR) data from near the middle of the clay at Wilson Lake, which suggests a lower sedimentation rate [110]. However, a closer inspection of these rates shows that they are in fact compatible with very rapid deposition of the base of the Marlboro Clay where foraminifera are extremely rare. Near the mid-point of the Marlboro Clay, the foraminifera abundance is approximately 200 specimens g^{-1} of sediment [110]. Using numerous lines of evidence, Stassen *et al*. [110] suggest that the sedimentation rate for this part of the Marlboro Clay is approximately 16 cm kyr^{-1}. Taking these two at face value, the corresponding foraminifera accumulation rate is approximately 4.5 individuals g^{-1} yr^{-1} (assuming sediment bulk density of 1.4, foraminifera density of 2.4 and average diameter of 150 µm). Independently, to match Stassen *et al.*'s [110] 16 cm kyr^{-1} sedimentation rate using the oligotrophic rate of 5 individuals cm^{-2} yr^{-1} of Žaric *et al.* [122], we expect approximately 223 individuals per gram of sediment, very close to the value computed above. Importantly, if we apply this foraminifera MAR to the abundances observed near the base of the clay (between 1 and 3 individuals g^{-1}) we arrive at a sedimentation rate of the order of several metres per thousand years, or *ca* 2 cm yr^{-1} at *ca* 1.6 individuals g^{-1}. This rate is consistent with Wright & Schaller's [19] estimate of 1.8 cm yr^{-1} and a decadal scale CIE onset. It is important to note that the oligotrophic rates of Zaric *et al*. [122] cited above are much lower than the mid-Atlantic shelf rate of approximately 70 individuals cm^{-2} yr^{-1} from the same study. At the latter rate the foraminiferal abundance in the middle of the clay is consistent with a high sedimentation rate, so it is clear that the potential foraminifera MARs in the Marlboro Clay deserve significant future attention.

The discussion above makes it apparent that these unusual hyperpycnal or mud-wave-type deposits on the inner shelf are unlikely to be geochemically or hydrographically equilibrated with

the open ocean. The foraminiferal 'barren zone' observed on the shelf is likely to be a product of simple dilution by a massive amount of rapidly deposited terrigenous sediment. The very limited foraminifera found in this interval, though small, are well preserved, which is unexpected if the barren interval was due to acidification of the shelves but consistent with marine organisms adapting to novel estuarine conditions brought about by sediment-laden freshwater input. We conclude that records from high sedimentation rate sites on the shelf, when viewed with coarse resolution, appear misleadingly similar to the open ocean, but in higher resolution offer a more nuanced picture of the sequence of events at the P-E boundary at a level of detail that will require a thorough application of shelf processes.

(d) Palaeocene–Eocene spherule chemistry and source of carbon for the onset of the carbon isotope excursion

Working under the hypothesis that the impact played some role in the onset of the CIE, we consider the possible sources of carbon for the onset alone. The P-E spherules generally have high CaO contents (approx. 20–35%, figure 4) compared with the impact ejecta from other known strewn fields. This is indicative of a target rock rich in $CaCO_3$, which upon vaporization would contribute carbon to the atmosphere. We have analysed the spherules for the typical trace elements that would be found in marine carbonate rocks (e.g. Sr). Although beyond the scope of this paper (and discussed in detail in [123]), we found that the bulk glass of the spherules has a Sr/Ca ratio between 0.15% and 0.3% measured by laser ablation-inductively coupled plasma mass spectrometry (LA-ICPMS) at RPI. Cenozoic marine carbonates have Sr/Ca ratios of 0.1–0.4% [124] because Sr is a favourable lattice substitution for Ca, pointing to a $CaCO_3$ source rock for the spherules. Therefore, we suggest that the target rocks contained a significant proportion of $CaCO_3$, probably as marine carbonates (of unknown age), and that this could represent a nearly instantaneous addition of carbon to the atmosphere. The Ca^{2+} would solidify or condense along with the other rock-forming elements of the target, while the CO_2 would remain volatilized.

The $\delta^{13}C$ value of typical shallow marine carbonates is between 0‰ and 5‰. There is no isotope effect from vaporization, hence the $CaCO_3$ carbon released by an impact would tend to make the $\delta^{13}C$ of atmospheric CO_2 higher than the presumed pre-event value of approximately −5‰. The addition of sufficient isotopically heavier C would still increase global temperatures and acidify the oceans, but would not be detectable using $\delta^{13}C$ alone as an indicator. However, if some amount of cometary carbon (average −40‰ to −60‰ [125]) were added to the pool of vaporized $CaCO_3$ carbon, the net effect could be a mixture of CO_2 with a $\delta^{13}C$ value somewhere between these two end-members. This would easily satisfy the onset of the excursion with whatever isotope value is desired to meet the observations (e.g. [64]), and the problem could be inverted to determine the necessary input $\delta^{13}C$. Such a release would decay very rapidly (decades to centuries). However, if the impact were a trigger for (or even simply coincident with) the contemporaneous addition of carbon from other reservoirs (discussed below), those sources could combine to produce the globally observed CIE.

Importantly, for the reasons above, we do not argue that the impact is responsible for the bulk of the carbon needed to generate the approximately 170 kyr event (onset through recovery) observed globally [23]. This is a truly colossal amount of carbon [126] and very unlikely to be sourced from a target rock or impactor alone. We merely suggest that the impact was most likely responsible for the initial onset of the excursion, which was followed shortly by multiple accompanying (and much more sluggish) additions of carbon from various Earth reservoirs. These sources could be the rapid eruption of the NAIP and/or intrusion of hydrocarbon reservoirs [15], dissociation of methane clathrates [12,13], or any number of other available reservoirs.

The precise emissions scenario is somewhat arbitrary, but our suggestion is by no means implausible. In fact, Gutjahr *et al*. [126] gives one modelling scenario with a *ca* 100 year or so initial release of carbon that is similar to what we suggest may have happened at the P-E

boundary, where a rapid initiation was followed by much slower and more protracted additions of a significant amount of carbon (over centuries to millennia). In the Gutjahr *et al*. scenario, the initial C released was quite negative, and subsequent emissions averaged out to be *ca* −12‰, but the overall effect of the onset rate was trivial. A framework for satisfying the globally observed requirements, and even a pulsed rapid-emissions scenario, was given by Kirtland Turner & Ridgwell [64], but a fast initial release has otherwise received only cursory attention.

We propose an easily testable scenario (and make other predictions that should be observable) if a more nuanced release schedule is applied to the onset and body of the P-E CIE. Because we are not modellers it is incumbent upon the modelling community to evaluate scenarios that realistically incorporate these difficult observations. The basic parameters are easily determined from our discussion above, but, until the Gutjahr *et al*. [126] paper, it has not been seriously considered. Our hope is that the scenario above will provide a starting point for a constructive advance.

(e) Climate change, carbon release and extraterrestrial impacts

Many extraterrestrial impacts had no apparent climatic consequence, while others have had environmental repercussions to varying degrees. No climate change appears to be associated with the approximately 35.4 Ma [127–129] Chesapeake Bay impact, but the potential climate effects of the approximately 35.7 Ma [130] Popigai impact are discussed below. The most obvious example of climate effects is the K-Pg impact [131,132], which coincided with a major mass extinction. The catalyst for the association between the Cretaceous–Palaeogene impact event and the K-Pg mass extinction was an anomalous layer at the K-Pg boundary with an unusually high concentration of Ir and other siderophile elements [132]. Though the crater was not found until many years later [133], the mass extinction at the K-Pg boundary (approx. 66 Ma) is now largely believed to be the result of the impact of a greater than 10 km body, although additional mechanisms may have played an important role in the severe environmental perturbations (see discussion on volcanism below [134,135]).

Rapid negative $\delta^{13}C$ excursions in marine sedimentary rocks are found coincident with the K-Pg extinction events, though these are probably not explicitly due to a release of C, and have been attributed to a severe biomass reduction and low marine productivity, dubbed the 'Strangelove' oceans [136]. Specifically, a negative $\delta^{13}C$ shift recorded by planktonic foraminifera and bulk $CaCO_3$ at the K-Pg boundary section in Agost, Spain, is attributed to a loss of pelagic biogenic $CaCO_3$ deposition [137], especially extinction of both planktonic foraminifera and calcareous nannoplankton [138,139]. The pronounced negative $\delta^{13}C$ excursion suggests an interruption of marine productivity and the ocean's biological pump, leading to a homogenized top to bottom water column [140]. Although there probably was an instantaneous release of carbon at the K-Pg [141] and protracted ocean acidification [142], the carbon would have been sourced from carbonate target rocks with a high $\delta^{13}C$ [143]. Intriguingly, new evidence suggests that the warming following the K-Pg impact was likely to have been faster than the anthropogenic rate [144]. A more protracted carbon degassing effect at the Chicxulub impact may be from an acceleration of Deccan volcanism that ramped up as a consequence of the impact [134] (see discussion below).

Other impacts in Earth's history have resulted in a CIE and subsequent warming, although these relationships have been given relatively little attention. A good example of a small hyperthermal and CIE [145] is the Popigai impact (Siberia), marked by the CPX strewn field [39,53,146] (preceding the North American strewn field and Chesapeake Bay impact [147]). Accompanying this event was a small *ca* 0.5‰ $\delta^{13}C$ excursion, whose origin could be an impact-induced release of carbon.

(f) Increased volcanism triggered by the Palaeocene–Eocene impact?

The exact trigger for enormous episodes of synchronous magmatism, such as the production of Large Igneous Provinces (LIPs), is not known. A growing body of evidence suggests

that magmatism in general can be induced or accelerated by external mechanisms like an extraterrestrial impact event [134,148–150]. For example, there is an observed connection between K-Pg impact and an increase in both mid-ocean ridge spreading rates [135] and a pulse of magmatism from the Deccan LIP [134,150]. The relationship between the Chicxulub impact and the Deccan is particularly intriguing, as it is directly analogous to the events at the P-E boundary: an extraterrestrial impact amidst the ongoing eruption of a LIP.

The Deccan Traps is a continental flood basalt with a total eruptive volume of greater than 1.3 million km^3 of lava [151], and temporally encompasses the K-Pg boundary. We know that impact-induced partial melting was not responsible for initiating the eruptions because Deccan extrusives predate the K-Pg impact by approximately 250 kyr [152]. However, recent high-precision ^{40}Ar-^{39}Ar dates of plagioclases from the most voluminous Kalsubai and Wai subgroups of the Deccan lava pile compared with dates of the Chicxulub melt rocks demonstrate a temporal coincidence between the K-Pg boundary impact and an acceleration of Deccan Traps volcanism [134]. These ^{40}Ar-^{39}Ar data coupled with high-precision U/Pb dates [152] and lava volume estimates [150] implicate the Chicxulub impact event in triggering a doubling of the extrusive rate somewhere within a 50 kyr time frame (this window is a function of the error on the ^{40}Ar-^{39}Ar dates) [134]. Furthermore, approximately 70% of the total Deccan Traps volcanism was erupted following the shift in eruption state that coincides with the K-Pg, possibly triggered by the strong seismic waves produced by the Chicxulub impact [134,150].

In a similar vein, a transient increase in mid-ocean ridge (MOR) production is reported at the K-Pg [135]. These findings are supported by an anomalous K-Pg-aged seafloor and global distribution of free-air gravity anomalies dated within a million years of the Chicxulub impact, both of which are attributed to impact-induced enhanced seismic activity [135]. The increase in MOR spreading rates would have led to a transient increase in degassing, contributing to the climate effects at the K-Pg. Though controversial, these studies suggest that the two mechanisms, extraterrestrial impacts and enhanced magmatism, should not be considered in isolation, and that they may be generalized to other such demonstrated temporal associations.

The NAIP began erupting in the late Palaeocene [153], but radiometric dates on a few intrusive complexes are basically coincident with the P-E boundary and the age of the P-E impact ejecta [14]. It is conceivable that the two events are related and that the P-E impact triggered an acceleration of NAIP volcanism similar to that argued for at the K-Pg and Deccan. Such acceleration would easily provide the additional carbon necessary to account for the bulk of the long CIE observed globally, as has been suggested by Gutjahr *et al*. [126]. The eruption of other LIPs has been shown to dramatically increase atmospheric pCO_2 through rapid degassing of extensive continental extrusives [154,155], making an observable atmospheric effect very likely. An atmospheric carbon input due to impact-induced acceleration of NAIP volcanism is consistent with all observations at the P-E boundary, making it a compelling target for future modelling work.

6. Summary

We have reviewed the lines of evidence for an extraterrestrial impact at the P-E boundary and speculated on its potential role in climate change. Those lines of evidence are: (i) glass spherules clearly shown to be air-fall ejecta, stratigraphically within the CIE onset now identified at five locations; (ii) shocked quartz grains and inclusions within the spherules; (iii) an Ir anomaly found at Zumaya, Spain; (iv) substantial charcoal and magnetic nanoparticles deposited stratigraphically following the ejecta layer; (v) a radiometric cooling age of the ejecta that is coincident with depositional age (a specific prediction of ejecta); and (vi) a plausible link between an impact event and increased volcanism in the early Eocene. Our preliminary data demonstrate that P-E spherules can be radiometrically dated, providing: (i) a potentially isochronous horizon at the P-E boundary; and (ii) evidence that the spherules are unlikely to be reworked Cretaceous–Palaeogene (K-Pg) ejecta, which is also supported by the presence of coeval spherules in the coastal plain and at open ocean Site 1051 (*ca* 2000 m water depth). Because the ejecta may be radiometrically dated, they will hopefully provide a source for an exact age of the boundary,

which is currently estimated using cyclostratigraphy [57,58] to interpolate between the CIE and dated ashes from several localities [14,59], none of which are precisely within the CIE onset. The search for P-E spherules at additional sites is currently underway and will aid in the quest for the crater location. We also suspect that ejecta should be found at sites where an Ir anomaly has been identified (Zumaya, Spain).

Although the CIE onset represents the initiation of global climate change at the P-E boundary, the ejecta spherules are consistent with air fall and may therefore represent a nearly instantaneous stratigraphic horizon to which all other observations at the boundary can be referenced. For example, it appears that the CIE recorded on the shelf is diachronous to some degree, which is either a function of differential reservoir response time or a consequence of diagenesis, indicating that the CIE (particularly in bulk carbonate) should not be used for assessing time scales or evaluating global response to a carbon cycle perturbation. The P-E boundary has rarely been scrutinized in such detail, and to have a marker that may be used as 'time-0' means that we are relieved of the burden of relying on the CIE onset to define the stratigraphic reference frame. This opens up new possibilities of assessing the true leads–lags in C-system response between different surficial carbon reservoirs that react and equilibrate on different time scales, which are compelling Earth System modelling targets. However, it is also apparent that the available foraminifera isotope data at P-E boundary sections on the North American Atlantic Coastal Plain are presently insufficient to take full advantage of this possibility.

We also outline a rough emissions scenario as a testable hypothesis: a rapid onset caused by the fast release of a mix of vaporized carbonate rock and cometary carbon, followed by additional degassing from an acceleration of the NAIP eruption rate. A sustained atmospheric carbon input due to impact-induced acceleration of NAIP volcanism is consistent with all observations at the P-E boundary, and analogous to the circumstances at the K-Pg transition, making it a compelling scenario for the ultimate origin of the event.

The first solid evidence of an extraterrestrial impact at the P-E boundary raises many questions: Where did it hit? How big was it? What were the ultimate consequences? We have only touched upon these questions here, but our results will no doubt spur numerous fruitful endeavours for years to come. The alternative to all the above arguments is that the impact was simply an unrelated coincidence with the P-E carbon release, isotope excursion, wildfires, massive deluge of continental sediments, NAIP volcanism, and global warming, having no actual effect itself. If that is the case at the P-E boundary, the same could be argued for any impact, such as the K-Pg; the causality similarly ascribed to that event is by simple association. However, at the P-E the dated impact spherules are found within the onset of the CIE and are the only physical evidence of a proposed trigger for the P-E boundary with demonstrated stratigraphic superposition with the event itself. That would indeed be a remarkable coincidence and we find it exceedingly unlikely.

Data accessibility. This article has no additional data.

Authors' contributions. M.F.S. and M.K.F. generated the data and wrote the paper.

Competing interests. The authors declare that they have no competing interests.

Funding. Source of funding for M.F.S. and M.K.F. is NSF award 1737100; M.K.F. was also funded by the Comer Science and Education Foundation.

Acknowledgements. We thank Dennis Kent and Jim Wright for many helpful discussions, Mimi Katz for her always helpful edits, and Charlie Langmuir for his suggestion to look for Sr in the spherules, and to Paul Pearson and an anonymous reviewer for their constructive comments that ultimately resulted in a much stronger manuscript. We thank Jared Singer for his assistance on the electron microprobe and laser ICMPS.

References

1. Gradstein FM, Ogg JG. 2012 Chapter 2—The chronostratigraphic scale. In *The geologic time scale* (eds FM Gradstein, JG Ogg, M Schmitz, G Ogg), pp. 31–42. Boston, MA: Elsevier.
2. Aubry M-P, Ouda K, Dupuis C, Berggren WA, Couvering JA. 2007 The Global Standard Stratotype-section and Point (GSSP) for the base of the Eocene Series in the Dababiya section (Egypt). *Episodes* **30**, 271–286.

3. Kennett JP, Stott LD. 1991 Abrupt deep-sea warming, palaeoceanographic changes and benthic extinctions at the end of the Palaeocene. *Nature* **353**, 225–229. (doi:10.1038/353225a0)
4. Koch PL, Zachos JC, Gingerich PD. 1992 Correlation between isotope records in marine and continental carbon reservoirs near the Palaeocene/Eocene boundary. *Nature* **358**, 319–322. (doi:10.1038/358319a0)
5. Kahn A, Aubry M-P. 2004 Provincialism associated with the Paleocene/Eocene thermal maximum: temporal constraint. *Mar. Micropaleontol.* **52**, 117–131. (doi:10.1016/j.marmicro.2004.04.003)
6. Kelly DC, Bralower TJ, Zachos JC, Silva IP, Thomas E. 1996 Rapid diversification of planktonic foraminifera in the tropical Pacific (ODP Site 865) during the late Paleocene thermal maximum. *Geology* **24**, 423–426. (doi:10.1130/0091-7613(1996)024<0423:RDOPFI>2.3.CO;2)
7. Crouch EM, Dickens GR, Brinkhuis H, Aubry M-P, Hollis CJ, Rogers KM, Visscher H. 2003 The Apectodinium acme and terrestrial discharge during the Paleocene-Eocene thermal maximum: new palynological, geochemical and calcareous nannoplankton observations at Tawanui, New Zealand. *Palaeogeogr. Palaeoclimatol. Palaeoecol.* **194**, 387–403. (doi:10.1016/S0031-0182(03)00334-1)
8. Wing SL, Harrington GJ, Smith FA, Bloch JI, Boyer DM, Freeman KH. 2005 Transient floral change and rapid global warming at the Paleocene-Eocene boundary. *Science* **310**, 993–996. (doi:10.1126/science.1116913)
9. Sluijs A *et al.* 2007 Environmental precursors to rapid light carbon injection at the Palaeocene/Eocene boundary. *Nature* **450**, 1218–1221. (doi:10.1038/nature06400)
10. Zachos JC *et al.* 2005 Rapid acidification of the ocean during the Paleocene-Eocene thermal maximum. *Science* **308**, 1611–1615. (doi:10.1126/science.1109004)
11. McInerney FA, Wing SL. 2011 The Paleocene-Eocene thermal maximum: a perturbation of carbon cycle, climate, and biosphere with implications for the future. *Annu. Rev. Earth Planet. Sci.* **39**, 489–516.
12. Dickens GR, O'Neil JR, Rea DK, Owen RM. 1995 Dissociation of oceanic methane hydrate as a cause of the carbon isotope excursion at the end of the Paleocene. *Paleoceanography* **10**, 965–971. (doi:10.1029/95PA02087)
13. Katz ME, Pak DK, Dickens GR, Miller KG. 1999 The source and fate of massive carbon input during the latest Paleocene thermal maximum. *Science* **286**, 1531–1533. (doi:10.1126/science.286.5444.1531)
14. Storey M, Duncan RA, Swisher CC. 2007 Paleocene-Eocene thermal maximum and the opening of the northeast Atlantic. *Science* **316**, 587–589. (doi:10.1126/science.1135274)
15. Svensen H, Planke S, Malthe-Sørenssen A, Jamtveit B, Myklebust R, Eidem TR, Rey SS. 2004 Release of methane from a volcanic basin as a mechanism for initial Eocene global warming. *Nature* **429**, 542–545. (doi:10.1038/nature02566)
16. Kent DV, Cramer BS, Lanci L, Wang D, Wright JD, Van Der Voo R. 2003 A case for a comet impact trigger for the Paleocene/Eocene thermal maximum and carbon isotope excursion. *Earth Planet. Sci. Lett.* **211**, 13–26. (doi:10.1016/S0012-821X(03)00188-2)
17. Cramer BS, Kent DV. 2005 Bolide summer: the Paleocene/Eocene thermal maximum as a response to an extraterrestrial trigger. *Palaeogeogr. Palaeoclimatol. Palaeoecol.* **224**, 144–166. (doi:10.1016/j.palaeo.2005.03.040)
18. Schaller MF, Fung MK, Wright JD, Katz ME, Kent DV. 2016 Impact ejecta at the Paleocene-Eocene boundary. *Science* **354**, 225–229. (doi:10.1126/science.aaf5466)
19. Wright JD, Schaller MF. 2013 Evidence for a rapid release of carbon at the Paleocene-Eocene thermal maximum. *Proc. Natl Acad. Sci. USA* **110**, 15 908–15 913. (doi:10.1073/pnas.1309188110)
20. Stassen P, Speijer RP, Thomas E. 2014 Unsettled puzzle of the Marlboro clays. *Proc. Natl Acad. Sci. USA* **111**, E1066–E1067. (doi:10.1073/pnas.1321839111)
21. Wright JD, Schaller MF. 2014 Reply to Pearson and Nicholas, Stassen *et al*. and Zeebe *et al*.: Teasing out the missing piece of the PETM puzzle. *Proc. Natl Acad. Sci. USA* **111**, E1068–E1071. (doi:10.1073/pnas.1321876111)
22. Pearson PN, Nicholas CJ. 2014 Layering in the Paleocene/Eocene boundary of the Millville core is drilling disturbance. *Proc. Natl Acad. Sci. USA* **111**, E1064–E1065. (doi:10.1073/pnas.1322077111)

23. Röhl U, Westerhold T, Bralower TJ, Zachos JC. 2007 On the duration of the Paleocene-Eocene thermal maximum (PETM). *Geochem. Geophys. Geosyst.* **8**, 1–13. (doi:10.1029/2007GC001784)
24. Glass BP. 1974 Microtektite surface sculpturing. *Geol. Soc. Am. Bull.* **85**, 1305–1314. (doi:10.1130/0016-7606(1974)85<1305:MSS>2.0.CO;2)
25. Glas, B. 1990 Tektites and microtektites: key facts and inferences. *Tectonophysics* **171**, 393–404. (doi:10.1016/0040-1951(90)90112-L)
26. Glass B, Burns CA. 1988 Microkrystites—a new term for impact-produced glassy spherules containing primary crystallites. In *Proc. 18th Lunar and Planetary Science Conference, Houston, TX, 16–20 March 1987*, pp. 455–458. Houston, TX: Lunar and Planetary Institute.
27. Stöffler D. 1984 Glasses formed by hypervelocity impact. *J. Non Cryst. Solids* **67**, 465–502. (doi:10.1016/0022-3093(84)90171-6)
28. Stöffler D, Langenhorst F. 1994 Shock metamorphism of quartz in nature and experiment: I. Basic observation and theory. *Meteoritics* **29**, 155–181. (doi:10.1111/j.1945-5100.1994.tb00670.x)
29. Miller KG *et al.* 2017 Wilson Lake site. In Proc. of the Ocean Drilling Program, Initial Reports, 174AX (Suppl.) (eds KG Miller *et al.*). College Station, TX: Ocean Drilling Program. See https://doi.org/10.2973/odp.proc.174AXS.111.2017.
30. Sugarman PJ *et al.* 2005 5. Millville site. In *Proceedings of the Ocean Drilling Program, initial reports* (eds KG Miller, PJ Sugarman, JV Browning *et al.*). College Station, TX: Ocean Drilling Program.
31. Kent DV *et al.* 2017 Deposition of pyromagnetically-enhanced Marlboro Clay offset from spherule peak at onset of CIE and Paleocene-Eocene boundary at the midshelf Millville core site (NJ Coastal Plain). In *Geological Society of America Fall Meeting Abstracts, New Orleans, LA, 11–15 December 2017*. Boulder, CO: Geological Society of America.
32. Kopp RE, Schumann D, Raub TD, Powars DS, Godfrey LV, Swanson-Hysell NL, Maloof AC, Vali H. 2009 An Appalachian Amazon? Magnetofossil evidence for the development of a tropical river-like system in the mid-Atlantic United States during the Paleocene-Eocene thermal maximum. *Paleoceanography* **24**, PA4211. (doi:10.1029/2009PA001783)
33. Norris R, Kroon D, Klaus A. 1998 Blake Nose paleoceanographic transect, western North Atlantic. In *Proc. of the Ocean Drilling Program, Initial reports*. College Station, TX: Ocean Drilling Program.
34. Liu S, Glass BP, Kyte FT, Bohaty SM. 2009 The late Eocene clinopyroxene-bearing spherule layer: new sites, nature of the strewn field, Ir data, and discovery of coesite and shocked quartz. *Geol. Soc. Am. Spec. Pap.* **452**, 37–70. (doi:10.1130/2009.2452(04))
35. Poag CW. 1997 The Chesapeake Bay bolide impact: a convulsive event in Atlantic Coastal Plain evolution. *Sediment. Geol.* **108**, 45–90. (doi:10.1016/S0037-0738(96)00048-6)
36. Langenhorst F. 1996 Characteristics of shocked quartz in late Eocene impact ejecta from Massignano (Ancona, Italy): clues to shock conditions and source crater. *Geology* **24**, 487–490. (doi:10.1130/0091-7613(1996)024<0487:COSQIL>2.3.CO;2)
37. Glass BP, Liu S, Montanari A. 2004 Impact ejecta in upper Eocene deposits at Massignano, Italy. *Meteorit. Planet. Sci.* **39**, 589–597. (doi:10.1111/j.1945-5100.2004.tb00921.x)
38. Glass BP. 2002 Upper Eocene impact ejecta/spherule layers in marine sediments. *Chemie der Erde - Geochemistry* **62**, 173–196. (doi:10.1078/0009-2819-00017)
39. Glass BP, Huber H, Koeberl C. 2004 Geochemistry of Cenozoic microtektites and clinopyroxene-bearing spherules. *Geochim. Cosmochim. Acta* **68**, 3971–4006. (doi:10.1016/j.gca.2004.02.026)
40. Koeberl C. 1990 The geochemistry of tektites: an overview. *Tectonophysics* **171**, 405–422. (doi:10.1016/0040-1951(90)90113-M)
41. Koeberl C. 1992 Tektite origin by hypervelocity asteroidal or cometary impact: target rocks, source craters, and mechanisms. *Geol. Soc. Am. Spec. Pap.* **293**, 133–152. (doi:10.1130/SPE293-p133)
42. Koeberl C, Beran A. 1988 Water content of tektites and impact glasses and related chemical studies. In *Proc. 18th Lunar and Planetary Science Conference, Houston, TX, 16–20 March 1987*, pp. 403–408. Houston, TX: Lunar and Planetary Institute.
43. Beran A, Koeberl C. 1997 Water in tektites and impact glasses by Fourier-transformed infrared spectrometry. *Meteorit. Planet. Sci.* **32**, 211–216. (doi:10.1111/j.1945-5100.1997.tb01260.x)

44. Melosh H, Artemieva N. 2004 How does tektite glass lose its water? *Lunar Planet. Sci.* XXXV, 1723.
45. Parkin D, Sullivan R, Andrews J. 1980 Further studies on cosmic spherules from deep-sea sediments. *Phil. Trans. R. Soc. Lond. A* **297**, 495–518. (doi:10.1098/rsta.1980.0227)
46. Glass BP, Simonson BM. 2012. *Distal impact ejecta layers: a record of large impacts in sedimentary deposits*. Berlin, Germany: Springer Science & Business Media.
47. Stöffler D, Ryder G, Ivanov BA, Artemieva NA, Cintala MJ, Grieve RA. 2006 Cratering history and lunar chronology. *Rev. Mineral. Geochem.* **60**, 519–596. (doi:10.2138/rmg.2006.60.05)
48. Gratz AJ, Fisler DK, Bohor BF. 1996 Distinguishing shocked from tectonically deformed quartz by the use of the SEM and chemical etching. *Earth Planet. Sci. Lett.* **142**, 513–521. (doi:10.1016/0012-821X(96)00099-4)
49. McMillan PF, Wolf GH, Lambert P. 1992 A Raman spectroscopic study of shocked single crystalline quartz. *Phys. Chem. Miner.* **19**, 71–79. (doi:10.1007/BF00198604)
50. Vonhof H, Smit J. 1999 Late Eocene microkrystites and microtektites at Maud Rise (Ocean Drilling Project Hole 689B; Southern Ocean) suggest a global extension of the approximately 35.5 Ma Pacific impact ejecta strewn field. *Meteorit. Planet. Sci.* **34**, 747–755. (doi:10.1111/j.1945-5100.1999.tb01387.x)
51. John C, Glass BP. 1974 Clinopyroxene-bearing glass spherules associated with North American microtektites. *Geology* **2**, 599–602. (doi:10.1130/0091-7613(1974)2<599:CGSAWN>2.0.CO;2)
52. Glass B, Burns CA, Crosbie JR, DuBois DL. 1985 Late Eocene North American microtektites and clinopyroxene-bearing spherules. *J. Geophys. Res. Solid Earth* **90**(S01), 175–196. (doi:10.1029/JB090iS01p00175)
53. Liu S, Papanastassiou DA, Ngo HH, Glass BP. 2006 Sr and Nd analyses of upper Eocene spherules and their implications for target rocks. *Meteorit. Planet. Sci.* **41**, 705–714. (doi:10.1111/j.1945-5100.2006.tb00986.x)
54. Bermúdez HD *et al.* 2016 The Cretaceous–Palaeogene boundary at Gorgonilla Island, Colombia, South America. *Terra Nova* **28**, 83–90. (doi:10.1111/ter.12196)
55. D'Hondt SL, Keller G, Stallard RF. 1987 Major element compositional variation within and between different late Eocene microtektite strewnfields. *Meteoritics* **22**, 61–79. (doi:10.1111/j.1945-5100.1987.tb00884.x)
56. Thomas DJ, Zachos JC, Bralower TJ, Thomas E, Bohaty S. 2002 Warming the fuel for the fire: evidence for the thermal dissociation of methane hydrate during the Paleocene-Eocene thermal maximum. *Geology* **30**, 1067–1070. (doi:10.1130/0091-7613(2002)030<1067:WTFFTF>2.0.CO;2)
57. Westerhold T, Röhl U, Laskar J. 2012 Time scale controversy: accurate orbital calibration of the early Paleogene. *Geochem. Geophys. Geosyst.* **13**, Q06015. (doi:10.1029/2012GC004096)
58. Westerhold T, Röhl U, Mccarren HK, Zachos JC. 2009 Latest on the absolute age of the Paleocene–Eocene Thermal Maximum (PETM): new insights from exact stratigraphic position of key ash layers +19 and −17. *Earth Planet. Sci. Lett.* **287**, 412–419. (doi:10.1016/j.epsl.2009.08.027)
59. Charles AJ, Condon DJ, Harding IC, Pälike H, Marshall JE, Cui Y, Kump L, Croudace IW. 2011 Constraints on the numerical age of the Paleocene-Eocene boundary. *Geochem. Geophys. Geosyst.* **12**, Q0AA17. (doi:10.1029/2010gc003426)
60. Renne PR, Swisher CC, Deino AL, Karner DB, Owens TL, Depaolo DJ. 1998 Intercalibration of standards, absolute ages and uncertainties in 40Ar/39Ar dating. *Chem. Geol.* **145**, 117–152. (doi:10.1016/S0009-2541(97)00159-9)
61. Jaramillo C *et al.* 2010 Effects of rapid global warming at the Paleocene-Eocene boundary on neotropical vegetation. *Science* **330**, 957–961. (doi:10.1126/science.1193833)
62. Schaller MF *et al.* Submitted. 40Ar-39Ar ages of the Paleocene-Eocene impact ejecta spherules. *Geophys. Res. Lett.*
63. Schaller MF, Fung MK, Turrin B. 2018 The extraterrestrial impact at the Paleocene-Eocene boundary carbon isotope excursion. In *Goldschmidt Abstracts, Boston, MA 12–17 August 2018*. Washington, DC: Geochemical Society.
64. Kirtland Turner S, Ridgwell A. 2016 Development of a novel empirical framework for interpreting geological carbon isotope excursions, with implications for the rate of

carbon injection across the PETM. *Earth Planet. Sci. Lett.* **435**, 1–13. (doi:10.1016/j.epsl.2015.11.027)
65. Chen C-T, Huang T-H, Chen Y-C, Bai Y, He X, Kang Y. 2013 Air-sea exchanges of CO2 in the world's coastal seas. *Biogeosciences* **10**, 6509. (doi:10.5194/bg-10-6509-2013)
66. Thomas H, Bozec Y, Elkalay K, De Baar HJ, Borges AV, Schiettecatte LS. 2005 Controls of the surface water partial pressure of CO2 in the North Sea. *Biogeosciences* **2**, 323–334. (doi:10.5194/bg-2-323-2005)
67. Thomas H, Bozec Y, Elkalay K, De Baar HJ. 2004 Enhanced open ocean storage of CO_2 from shelf sea pumping. *Science* **304**, 1005–1008. (doi:10.1126/science.1095491)
68. Kyte FT, Smit J. 1986 Regional variations in spinel compositions: an important key to the Cretaceous/Tertiary event. *Geology* **14**, 485–487. (doi:10.1130/0091-7613(1986)14<485:RVISCA>2.0.CO;2)
69. Pierrard O, Robin E, Rocchia R, Montanari A. 1998 Extraterrestrial Ni-rich spinel in upper Eocene sediments from Massignano, Italy. *Geology* **26**, 307–310. (doi:10.1130/0091-7613(1998)026<0307:ENRSIU>2.3.CO;2)
70. Robin E, Molina E. 2006 Chronostratigraphy, composition, and origin of Ni-rich spinel from the Late Eocene Fuente Caldera section in Spain: one impact or more? *Meteorit. Planet. Sci.* **41**, 1231–1248. (doi:10.1111/j.1945-5100.2006.tb00518.x)
71. Quitté G, Robin E, Levasseur S, Capmas F, Rocchia R, Birck JL, Allègre CJ. 2007 Osmium, tungsten, and chromium isotopes in sediments and in Ni-rich spinel at the K-T boundary: signature of a chondritic impactor. *Meteorit. Planet. Sci.* **42**, 1567–1580. (doi:10.1111/j.1945-5100.2007.tb00591.x)
72. Smit J, Kyte FT. 1984 Siderophile-rich magnetic spheroids from the Cretaceous–Tertiary boundary in Umbria, Italy. *Nature* **310**, 403. (doi:10.1038/310403a0)
73. Deer WA, Howie RA, Zussman J. 1996 *An introduction to the rock-forming minerals*, 2nd edn. London, UK: Longman.
74. Sack RO, Ghiorso MS. 1991 An internally consistent model for the thermodynamic properties of Fe–Mg-titanomagnetite-aluminate spinels. *Contrib. Mineral. Petrol.* **106**, 474–505. (doi:10.1007/BF00321989)
75. Vickery AM, Melosh HJ. 1990 Atmospheric erosion and impactor retention in large impacts, with application to mass extinctions. *Geol. Soc. Am. Spec. Pap.* **247**, 289–300. (doi:10.1130/SPE247-p289)
76. Dolenec T, Pavšič J, Lojen S. 2000 Ir anomalies and other elemental markers near the Palaeocene–Eocene boundary in a flysch sequence from the Western Tethys (Slovenia). *Terra Nova* **12**, 199–204. (doi:10.1046/j.1365-3121.2000.00292.x)
77. Schmitz B, Asaro F, Molina E, Monechi S, Von Salis K, Speijer RP. 1997 High-resolution iridium, δ13C, δ18O, foraminifera and nannofossil profiles across the latest Paleocene benthic extinction event at Zumaya, Spain. *Palaeogeogr. Palaeoclimatol. Palaeoecol.* **133**, 49–68. (doi:10.1016/S0031-0182(97)00024-2)
78. Schmitz B, Peucker-Ehrenbrink B, Heilmann-Clausen C, Åberg G, Asaro F, Lee CT. 2004 Basaltic explosive volcanism, but no comet impact, at the Paleocene–Eocene boundary: high-resolution chemical and isotopic records from Egypt, Spain and Denmark. *Earth Planet. Sci. Lett.* **225**, 1–17. (doi:10.1016/j.epsl.2004.06.017)
79. Montanari A, Asaro F, Michel HV, Kennett JP. 1993 Iridium anomalies of late Eocene age at Massignano (Italy), and ODP site 689B (Maud Rise, Antarctic). *Palaios* **8**, 420–437. (doi:10.2307/3515017)
80. Glass BP, Koeberl C. 2006 Australasian microtektites and associated impact ejecta in the South China Sea and the Middle Pleistocene supereruption of Toba. *Meteorit. Planet. Sci.* **41**, 305–326. (doi:10.1111/j.1945-5100.2006.tb00211.x)
81. Glass B, Pizzuto J. 1994 Geographic variation in Australasian microtektite concentrations: implications concerning the location and size of the source crater. *J. Geophys. Res. Planets* **99**(E9), 19 075–19 081. (doi:10.1029/94JE01866)
82. Sharpton V, Gibson Jr J. 1990 The Marquez Dome impact structure, Leon County, Texas. In *Abstracts of the Lunar and Planetary Science Conference* **21**, 1136–1137.
83. McHone J, Sorkhabi R. 1994 Apatite fission-track age of Marquez Dome impact structure, Texas. *Abstracts of the Lunar and Planetary Science Conference* **25**, 881–882.

84. Buchanan PC, Koeberl C, Reid AM. 1998 Impact into unconsolidated, water-rich sediments at the Marquez Dome, Texas. *Meteorit. Planet. Sci.* **33**, 1053–1064. (doi:10.1111/j.1945-5100.1998.tb01712.x)
85. Gibson JW. 1990 Marquez Dome: an impact feature in Leon County, Texas. PhD dissertation, Department of Geosciences, University of Houston, Houston, TX, USA.
86. Shuvalov VV. 2002 Radiation effects of the Chicxulub impact event. In *Geological and biological effects of impact events* (eds E Buffetaut *et al.*), pp. 237–247. Berlin, Germany: Springer.
87. Collins GS, Melosh HJ, Marcus RA. 2005 Earth impact effects program: a web-based computer program for calculating the regional environmental consequences of a meteoroid impact on Earth. *Meteorit. Planet. Sci.* **40**, 817–840. (doi:10.1111/j.1945-5100.2005.tb00157.x)
88. Wolbach WS, Lewis RS, Anders E. 1985 Cretaceous extinctions: evidence for wildfires and search for meteoritic material. *Science* **230**, 167–170. (doi:10.1126/science.230.4722.167)
89. Venkatesan M, Dahl J. 1989 Organic geochemical evidence for global fires at the Cretaceous/Tertiary boundary. *Nature* **338**, 57. (doi:10.1038/338057a0)
90. Melosh HJ, Schneider N, Zahnle K, Latham D. 1990 Ignition of global wildfires at the Cretaceous/Tertiary boundary. *Nature* **343**, 251. (doi:10.1038/343251a0)
91. Fung MK, Schaller MF, Hoff CM, Katz ME, Wright JD 2016 Widespread wildfires at the Paleocene–Eocene boundary: evidence from abundant charcoal preserved in the thick Marlboro Clay. In *Geological Society of America Fall Meeting Abstracts, Denver, CO, 25–28 September 2016*. Boulder, CO: Geological Society of America.
92. Lippert PC, Zachos JC 2007 A biogenic origin for anomalous fine-grained magnetic material at the Paleocene–Eocene boundary at Wilson Lake, New Jersey. *Paleoceanography* **22**, PA4104. (doi:10.1029/2007PA001471)
93. Makarova M, Wright JD, Miller KG, Babila TL, Rosenthal Y, Park JI. 2017 Hydrographic and ecologic implications of foraminiferal stable isotopic response across the US mid-Atlantic continental shelf during the Paleocene-Eocene Thermal Maximum. *Paleoceanography* **32**, 56–73. (doi:10.1002/2016PA002985)
94. Fung MK. 2017 Reconstructing paleoenvironments in the Paleogene: microfossils on the paleocontinental coastal plain. PhD dissertation, Department of Earth and Environmental Sciences., Rensselaer Polytechnic Institute, Troy, NY, USA.
95. Lanci L, Kent DV, Miller KG. 2002 Detection of Late Cretaceous and Cenozoic sequence boundaries on the Atlantic coastal plain using core log integration of magnetic susceptibility and natural gamma ray measurements at Ancora, New Jersey. *J. Geophys. Res.* **107**(B10), 2216. (doi:10.1029/2000JB000026)
96. Kent DV, Lanci L, Wang H, Wright JD. 2017 Enhanced magnetization of the Marlboro Clay as a product of soil pyrogenesis at the Paleocene–Eocene boundary? *Earth Planet. Sci. Lett.* **473**, 303–312. (doi:10.1016/j.epsl.2017.06.014)
97. Cannon SH, Gartner JE. 2005 Wildfire-related debris flow from a hazards perspective. In *Debris-flow hazards and related phenomena* (eds M Jakob, O Hungr), pp. 363–385. Berlin, Germany: Springer.
98. Swanson FJ. 1981 Fire and geomorphic processes. In *Fire regimes and ecosystem properties* (eds HA Mooney, TM Bonnicksen, NL Christensen, JE Lotan, WA Reiners), pp. 401–444. USDA Forest Service General Technical report WO-26. Washington, DC: USDA Forest Service.
99. Bains S, Corfield RM, Norris RD. 1999 Mechanisms of climate warming at the end of the Paleocene. *Science* **285**, 724–727. (doi:10.1126/science.285.5428.724)
100. Self-Trail JM *et al.* 2017 Shallow marine response to global climate change during the Paleocene-Eocene Thermal Maximum, Salisbury Embayment, USA. *Paleoceanography* **32**. 710–728. (doi:10.1002/2017PA003096)
101. Powars DS, Edwards LE, Kidwell SM, Schindler JS. 2015 Cenozoic stratigraphy and structure of the Chesapeake Bay region. *Field Guides* **40**, 171–229. (doi:10.1130/2015.0040(07))
102. Gibson T, Bybell L, Mason D. 2000 Stratigraphic and climatic implications of clay mineral changes around the Paleocene/Eocene boundary of the northeastern US margin. *Sediment. Geol.* **134**, 65–92. (doi:10.1016/S0037-0738(00)00014-2)
103. Gibson TG, Bybell LM, Owens JP. 1993 Latest Paleocene lithologic and biotic events in neritic deposits of southwestern New Jersey. *Paleoceanography* **8**, 495–514. (doi:10.1029/93PA01367)

104. Lamb MP, Mcelroy B, Kopriva B, Shaw J, Mohrig D. 2010 Linking river-flood dynamics to hyperpycnal-plume deposits: experiments, theory, and geological implications. *Geol. Soc. Am. Bull.* **122**, 1389–1400. (doi:10.1130/B30125.1)
105. Geyer WR, Hill P, Milligan T, Traykovski P. 2000 The structure of the Eel River plume during floods. *Cont. Shelf Res.* **20**, 2067–2093. (doi:10.1016/S0278-4343(00)00063-7)
106. Warrick JA, Melack JM, Goodridge BM. 2015 Sediment yields from small, steep coastal watersheds of California. *J. Hydrol. Reg. Stud.* **4**, 516–534. (doi:10.1016/j.ejrh.2015.08.004)
107. Warrick JA, Xu J, Noble MA, Lee HJ. 2008 Rapid formation of hyperpycnal sediment gravity currents offshore of a semi-arid California river. *Cont. Shelf Res.* **28**, 991–1009. (doi:10.1016/j.csr.2007.11.002)
108. Cramer BS, Aubry MP, Miller KG, Olsson RK, Wright JD, Kent DV. 1999 An exceptional chronologic, isotopic, and clay mineralogic record of the latest Paleocene thermal maximum, Bass River, NJ, ODP 174AX. *Bull. Géol. Soc. Fr.* **170**, 883–897.
109. Zeebe RE, Ridgwell A, Zachos JC. 2016 Anthropogenic carbon release rate unprecedented during the past 66 million years. *Nat. Geosci.* **9**, 325–329. (doi:10.1038/ngeo2681)
110. Stassen P, Thomas E, Speijer RP. 2012 Integrated stratigraphy of the Paleocene-Eocene thermal maximum in the New Jersey Coastal Plain: toward understanding the effects of global warming in a shelf environment. *Paleoceanography* **27**, PA4210. (doi:10.1029/2012PA002323)
111. Babila TL, Rosenthal Y, Wright JD, Miller KG. 2016 A continental shelf perspective of ocean acidification and temperature evolution during the Paleocene-Eocene Thermal Maximum. *Geology* **44**, 275–278. (doi:10.1130/G37522.1)
112. Wright J, Miller K. 2016 Foraminiferal stable isotope record at Millville, NJ: implications for the onset of the PETM. In *AGU Fall Meeting Abstracts, San Francisco, CA, 12–16 December 2016*. Washington, DC: American Geophysical Union.
113. Ito RG, Schneider B, Thomas H. 2005 Distribution of surface fCO2 and air–sea fluxes in the Southwestern subtropical Atlantic and adjacent continental shelf. *J. Mar. Syst.* **56**, 227–242. (doi:10.1016/j.jmarsys.2005.02.005)
114. Liu K-K, Atkinson L, Chen CT, Gao S, Hall J, Macdonald RW, McManus LT, Quinones R. 2000 Exploring continental margin carbon fluxes on a global scale. *Eos* **81**, 641–644. (doi:10.1029/EO081i052p00641-01)
115. Bohor BF. 1996 A sediment gravity flow hypothesis for siliciclastic units at the K/T boundary, northeastern Mexico. The Cretaceous Tertiary Event and Other Catastrophes in Earth History. *Geol. Soc. Am. Spec. Pap.* **307**, 183–195.
116. Bohor BF, Betterton WJ. 1993 Arroyo el Mimbral, Mexico, K/T unit: origin as debris flow/turbidite, not a tsunami deposit. *Abstracts of the Lunar and Planetary Science Conference* **23**, 143–144.
117. Swift D, Thorne J. 1991 Sedimentation on continental margins I: a general model for shelf sedimentation. *Shelf Sand and Sandstone Bodies* **14**, 3–31.
118. Posamentier HW, Jervey MT, Vail PR. 1988 Eustatic controls on clastic deposition. I. Conceptual framework. In *Sea level changes: an integrated approach* (eds CK Wilgus, BS Hastings, CGStC Kendall, HW Posamentier, CA Ross, JC Van Wagoner), pp. 110–124. SEPM Special Publication, vol. 42. Society of Economic Paleontologists and Mineralogists.
119. Stassen P, Thomas E, Speijer R. 2012 The progression of environmental changes during the onset of the Paleocene-Eocene thermal maximum (New Jersey Coastal Plain). *Austrian J. Earth Sci.* **105**, 169–178.
120. Pearson P, Thomas E. 2015 Drilling disturbance and constraints on the onset of the Paleocene–Eocene boundary carbon isotope excursion in New Jersey. *Clim. Past* **11**, 95–104. (doi:10.5194/cp-11-95-2015)
121. Podrecca L *et al.* 2017 Clear as mud: changes in paleoshelf environments and deposition rates at Medford, New Jersey during the Paleocene-Eocene Thermal Maximum. In *AGU Fall Meeting Abstracts, New Orleans, LA, 11–15 December 2017*. Washington, DC: American Geophysical Union.
122. Žarić S, Schulz M, Mulitza S. 2006 Global prediction of planktic foraminiferal fluxes from hydrographic and productivity data. *Biogeosciences* **3**, 187–207. (doi:10.5194/bg-3-187-2006)
123. Schaller MF, Fung MK. In preparation. Trace element geochemistry of the Paleocene-Eocene impact ejecta spherules.

124. Sosdian SM, Lear CH, Tao K, Grossman EL, O'Dea A, Rosenthal Y. 2012 Cenozoic seawater Sr/Ca evolution. *Geochem. Geophys. Geosyst.* **13**, Q10014. (doi:10.1029/2012GC004240)
125. Messenger S. 2000 Identification of molecular-cloud material in interplanetary dust particles. *Nature* **404**, 968. (doi:10.1038/35010053)
126. Gutjahr M, Ridgwell A, Sexton PF, Anagnostou E, Pearson PN, Pälike H, Norris RD, Thomas E, Foster GL. 2017 Very large release of mostly volcanic carbon during the Palaeocene–Eocene Thermal Maximum. *Nature* **548**, 573–577. (doi:10.1038/nature23646)
127. Deutsch A, Koeberl C. 2006 Establishing the link between the Chesapeake Bay impact structure and the North American tektite strewn field: the Sr-Nd isotopic evidence. *Meteorit. Planet. Sci.* **41**, 689–703. (doi:10.1111/j.1945-5100.2006.tb00985.x)
128. Glass B, Hall C, York D. 1986 40Ar/39Ar laser-probe dating of North American tektite fragments from Barbados and the age of the Eocene-Oligocene boundary. *Chem. Geol. Isot. Geosci. Sect.* **59**, 181–186. (doi:10.1016/0168-9622(86)90070-9)
129. Horton WJ, Izett GA. 2005 Crystalline-rock ejecta and shocked minerals of the Chesapeake Bay impact structure, USGS-NASA Langley core, Hampton, Virginia, with supplemental constraints on the age of impact. In *Studies of the Chesapeake Bay impact structure: the USGS-NASA Langley corehole, Hampton, Virginia and related coreholes and geophysical surveys* (eds JW Horton Jr, DS Powars, GS Gohn), ch. E, p. 30. US Geological Survey Professional Paper 1688. See https://pubs.usgs.gov/pp/2005/1688/ak/PP1688_chapE.pdf.
130. Bottomley R, Grieve R, York D, Masaitis V. 1997 The age of the Popigai impact event and its relation to events at the Eocene/Oligocene boundary. *Nature* **388**, 365. (doi:10.1038/41073)
131. Alvarez W, Asaro F, Michel HV, Alvarez LW. 1982 Iridium anomaly approximately synchronous with terminal Eocene extinctions. *Science* **216**, 886–888. (doi:10.1126/science.216.4548.886)
132. Alvarez LW, Alvarez W, Asaro F, Michel HV. 1980 Extraterrestrial cause for the Cretaceous-Tertiary extinction. *Science* **208**, 1095–1108. (doi:10.1126/science.208.4448.1095)
133. Hildebrand AR, Penfield GT, Kring DA, Pilkington M, Camargo ZA, Jacobsen SB, Boynton WV. 1991 Chicxulub crater: a possible Cretaceous/Tertiary boundary impact crater on the Yucatan Peninsula, Mexico. *Geology* **19**, 867–871. (doi:10.1130/0091-7613(1991)019<0867:CCAPCT>2.3.CO;2)
134. Renne PR, Sprain CJ, Richards MA, Self S, Vanderkluysen L, Pande K. 2015 State shift in Deccan volcanism at the Cretaceous-Paleogene boundary, possibly induced by impact. *Science* **350**, 76–78. (doi:10.1126/science.aac7549)
135. Byrnes JS, Karlstrom L. 2018 Anomalous K-Pg–aged seafloor attributed to impact-induced mid-ocean ridge magmatism. *Sci. Adv.* **4**, eaao2994. (doi:10.1126/sciadv.aao2994)
136. Hsu KJ, Oberhansli H, Gao JY, Shu S, Haihong C, Krahenbuhl U. 1985 'Strangelove ocean' before the Cambrian explosions. *Nature* **316**, 809–811.
137. Smit J. 1990 Meteorite impact, extinctions and the Cretaceous-Tertiary boundary. *Geol. Mijnbouw* **69**, 187–204.
138. Bown P. 2005 Selective calcareous nannoplankton survivorship at the Cretaceous-Tertiary boundary. *Geology* **33**, 653–656. (doi:10.1130/G21566.1)
139. MacLeod N *et al.* 1997 The Cretaceous-tertiary biotic transition. *J. Geol. Soc. London* **154**, 265–292. (doi:10.1144/gsjgs.154.2.0265)
140. Kump LR. 1991 Interpreting carbon-isotope excursions: Strangelove oceans. *Geology* **19**, 299–302. (doi:10.1130/0091-7613(1991)019<0299:ICIESO>2.3.CO;2)
141. Beerling DJ, Lomax BH, Royer DL, Upchurch GR, Kump LR. 2002 An atmospheric pCO2 reconstruction across the Cretaceous-Tertiary boundary from leaf megafossils. *Proc. Natl Acad. Sci. USA* **99**, 7836–7840. (doi:10.1073/pnas.122573099)
142. Tyrrell T, Merico A, McKay DIA. 2015 Severity of ocean acidification following the end-Cretaceous asteroid impact. *Proc. Natl Acad. Sci. USA* **112**, 6556–6561. (doi:10.1073/pnas.1418604112)
143. O'Keefe JD, Ahrens TJ. 1989 Impact production of CO_2 by the Cretaceous/Tertiary extinction bolide and the resultant heating of the Earth. *Nature* **338**, 247–249.
144. MacLeod KG, Quinton PC, Sepúlveda J, Negra MH. 2018 Postimpact earliest Paleogene warming shown by fish debris oxygen isotopes (El Kef. *Tunisia). Science* **360**, 1467–1469. (doi:10.1126/science.aap8525)

145. Pusz AE, Miller KG, Wright JD, Katz ME, Cramer BS, Kent DV. 2009 Stable isotopic response to late Eocene extraterrestrial impacts. *Geol. Soc. Am. Spec. Pap.* **452**, 83–95. (doi:10.1130/2009.2452(06))
146. Whitehead J, Papanastassiou DA, Spray JG, Grieve RA, Wasserburg GJ. 2000 Late Eocene impact ejecta: geochemical and isotopic connections with the Popigai impact structure. *Earth Planet. Sci. Lett.* **181**, 473–487. (doi:10.1016/S0012-821X(00)00225-9)
147. Glass B, Koeberl C, Blum JD, Mchugh CMG. 1998 Upper Eocene tektite and impact ejecta layer on the continental slope off New Jersey. *Meteorit. Planet. Sci.* **33**, 229–241. (doi:10.1111/j.1945-5100.1998.tb01628.x)
148. Rampino MR. 1987 Impact cratering and flood basalt volcanism. *Nature* **327**, 468.
149. Price NJ. 2001 *Major impacts and plate tectonics*. London, UK: Routledge.
150. Richards MA *et al.* 2015 Triggering of the largest Deccan eruptions by the Chicxulub impact. *Geol. Soc. Am. Bull.* **127**, 1507–1520. (doi:10.1130/B31167.1)
151. Jay AE, Widdowson M 2008 Stratigraphy, structure and volcanology of the SE Deccan continental flood basalt province: implications for eruptive extent and volumes. *J. Geol. Soc. London* **165**, 177–188.
152. Schoene B, Samperton KM, Eddy MP, Keller G, Adatte T, Bowring SA, Khadri SFR, Gertsch B. 2015 U-Pb geochronology of the Deccan Traps and relation to the end-Cretaceous mass extinction. *Science* **347**, 182–184. (doi:10.1126/science.aaa0118)
153. Storey M, Duncan RA, Tegner C. 2007 Timing and duration of volcanism in the North Atlantic Igneous Province: implications for geodynamics and links to the Iceland hotspot. *Chem. Geol.* **241**, 264–281. (doi:10.1016/j.chemgeo.2007.01.016)
154. Schaller MF, Wright JD, Kent DV, Olsen PE. 2012 Rapid emplacement of the Central Atlantic Magmatic Province as a net sink for CO2. *Earth Planet. Sci. Lett.* **323–324**, 27–39. (doi:10.1016/j.epsl.2011.12.028)
155. Schaller MF, Wright JD, Kent DV. 2011 Atmospheric pCO_2 perturbations associated with the Central Atlantic Magmatic Province. *Science* **331**, 1404–1409. (doi:10.1126/science.1199011)